Master's thesis

NTNU
Norwegian University of Science and Technology
Faculty of Information Technology and Electrical Engineering
Department of Electric Power Engineering

Ulrikke Bing

Microgrid Control: The impact of different control strategies on the system adequacy

Master's thesis in Energy and Environmental Engineering
Supervisor: Kjetil Uhlen
June 2020

NTNU
Norwegian University of Science and Technology

TrønderEnergi

Ulrikke Bing

Microgrid Control: The impact of different control strategies on the system adequacy

Master's thesis in Energy and Environmental Engineering
Supervisor: Kjetil Uhlen
June 2020

Norwegian University of Science and Technology
Faculty of Information Technology and Electrical Engineering
Department of Electric Power Engineering

NTNU
Norwegian University of
Science and Technology

Abstract

The world is facing a continuously growing energy demand at the same time as the climate changes demand a significant cut in greenhouse gas emissions. The inhabitants of Norway expect constant access to electricity, preferably generated by renewable power sources. To accommodate this TrønderEnergi is currently investigating the possibility of installing autonomous microgrid configurations containing renewable power sources and energy storage units at remote places with limited access to the utility grid.

In collaboration with the EU-funded REMOTE-project, TrønderEnergi has established a test site at Rye in Trøndelag. A 225 kW wind turbine and an 86.4 kWp PV-system has been installed to supply the farm Langørgen Øvre. These renewable resources have a fluctuating power production, and a 554 kWh battery energy storage system and a 1.67 MWh hydrogen energy storage system have been installed to ensure energy balance in the microgrid. Additionally, the grid is equipped with a backup diesel generator. The project has a goal of 98% availability.

Furthermore, a master-slave control strategy is implemented in the microgrid. The battery will serve as the master unit in the system, and the master controller ensures energy balance by administering the operation of the resources in the grid.

The objective of this thesis is to investigate the impact of different control strategies on the system adequacy of the microgrid. By utilising both an analytical method and Monte Carlo Simulations, the reliability indices LOLP, LOLE and EENS were calculated for each of the control strategies. The scores were thereby utilised to compare the adequacy performance of the cases.

The following list presents the control strategies used in the four cases:

- Case 1 - The control strategy implemented at Rye. A master-slave control strategy with the BESS as master unit.
- Case 2 - A master-slave control strategy with the BESS as master-unit and demand-side management available.
- Case 3 - A master-slave control strategy with both the BESS and the HESS as master-units.
- Case 4 - A peer-to-peer control strategy.

A MATLAB-model was developed for each of the cases, modelling the operation of the microgrid. Both consumption data from the farm and production data from the renewable

sources were used as input when modelling. In addition, simulated production data from RenewablesNinja was used to expand the amount of historical production data.

Based on the adequacy assessments performed, it was found that all four control strategies ensured an availability above 99%, reaching the reliability goal of the REMOTE-project. Nevertheless, only minor distinctions of adequacy performance were detected. Case 4 stood out as the case with the most unsatisfactory results. The peer-to-peer strategy does, however, benefit from the fact that no inter-unit-communication system or master controller is needed. These advantages were not accounted for in the calculated indices, and a discussion of how this impacted the results was conducted. Further, slightly better performance of case 3 could be detected. The results did, however, vary in the different simulations performed, and no clear conclusion could be drawn.

Consequently, the results presented in this thesis were not definite enough to conclude on which of the control strategies that ensure the best adequacy performance at Rye.

Sammendrag

Verden står ovenfor en kontinuerlig økende etterspørsel etter energi, samtidig som klimaendringene krever betydelige kutt i klimagassutslipp. Innbyggerne i Norge forventer nå konstant tilgang til strøm, og ettersom global oppvarming truer, skal den helst være generert av fornybare kilder. For å imøtekomme dette ønsket undersøker TrønderEnergi for tiden muligheten for å installere autonome mikronett bestående av fornybare energikilder og energilagringsenehter på fjerntliggende områder med begrenset tilgang til oppkobling på kraftnettet.

I samarbeid med det EU-finansierte REMOTE-prosjektet har TrønderEnergi etablert et pilotprosjekt på Rye i Trøndelag. Her er det satt opp en 225 kW vindturbin og et 86.4 kWp PV-system som skal forsyne gården Langørgen Øvre med energi. Energikildene er avhengig av værforhold og har dermed varierende produksjon. For å balansere ut energien i mikronettet er det derfor installert et 554 kWh stort batterilagringssystem og et hydrogenlagringsystem på 1.67 MWh. Prosjektet har et mål om 98% tilgjengelighet i mikronettet, og i tillegg til de fornybare kildene og lagringsenehetene er det nettet utstyrt med en bakcup-dieselgenerator.

Videre er det blitt implementer en master-slave-kontrollstrategi i nettet. Her vil batteriet fungere som "master" i systemet og være hovedansvarlig for å opprettholde riktig frekvens- og spenningsnivå. I tillegg vil en "master controller" ha hovedansvaret for energibalansen i systemt og administere de andre enhetene i nettet slik at denne blir opprettholdt.

Målet med denne masteroppgaven er å undersøke hvordan bruken av ulike kontrollstartegier påvirker påliteligheten til mikronettet på Rye. Ved hjelp av både en analytisk medtode og Monte Carlo simuleringer skal pålitelighetsindeksene LOLP, LOLE og EENS regnes ut for hver av kontrollstrategiene. Resulatene vil så gi gurnnlaget for en sammlinkning av påliteligheten til de forskjellige casene.

Følgende kontrollstrategier ble undersøkt:

- Case 1 - Kontrollstrategien allerede implementert på Rye. En master-slave-kontrollstrategi med batteriet som masterenhet.
- Case 2 - En master-slave-kontrollstrategi med batteriet som masterenhet og løsninger for fleksibel last tilgjengelig.
- Case 3 - En master-slave-kontrollstrategi med både batteriet og hydrogensystemet som master-enheter.
- Case 4 - En peer-to-peer kontrollstrategi.

For hver av de fire casene ble mikronettets drift og ytelse modellert i MATLAB. Både forbruksdata fra gården og produksjonsdata fra de fornybare kildene ble brukt som input i modellene. For å øke tilgangen på historisk produksjonsdata ble også simuleringverktøyet RenewablesNinja benyttet. Dette verktøyet ga ytteligere datasett med produksjonsdata.

Basert på undersøkelselse gjort ble det funnet at alle de fire kontrollstrategiene sikret en tilgjengelighet på over 99%, noe som tilsvarer at alle nådde målet satt for REMOTE-prsjektet. Forskjellene mellom de utregnede pålitelighetsindeksene var derimot små, og det var vanskelig å finne ut hvilke av de fire kontrollstrategiene som førte til best pålitelighet. Case 4 skilte seg noe ut, da de beregnede indeksene var litt høyere for denne kontrollstrategiene, sammenlinket med de andre. Peer-to-peer-strategien har imidlertid den fordelen at inget kommunikasjonsystsem som går på tvers av enheter eller en "master controller" er nødvendig. Dette er en fordel, da feil i disse kan føre til utfall når en benytter seg av en master-slave-stategi. Denne fordelen ble ikke tatt med i beregningen av indeksene og det ble argumentert for at case 4 dermed hadde noe bedre pålitelighet enn det indeksene viste. I tillegg ble det funnet at case 3 så ut til å ha noe økt pålitelighet sammenliknet med de andre casene. Resultatene var imidlertid såpass utydelige at ingen klar konklusjon kunne trekkes.

Det ble dermed konkludert med at ingen av de fire kontrollstrategiene virket å sikre en bedre pålitelighet. Dette var basert på resultatete lagt frem i denne oppgaven.

Acknowledgement

Gratitude goes to my family, friends and boyfriend for all the love, support and encouragement. You kept me sane through times of both social distancing and intense work. Thank you.

I would also like to thank my supervisor Kjetil Uhlen for great guidance and willingness to help throughout the semester. Your support and availability are highly appreciated.

Lastly, I would like to thank my contact persons in TrønderEnergi, Anniken Auke Borge and Bernhard Kvaal, for providing so much useful information and answering all of my questions.

Trondheim, June 2020
Ulrikke Bing
(U.B.)

Table of Contents

List of Tables

List of Figures

Abbreviations

REMOTE	=	Remote area Energy Supply with Multiple Options for integrated hydrogen-based TEchnologies
PV	=	PhotoVoltaic
MPP	=	Maximum Power Point
MPPT	=	Maximum Power Point Tracker
ESS	=	Energy Storage System
BESS	=	Battery Energy Storage System
HESS	=	Hydrogen Energy Storage System
SoC	=	State of Charge
DoD	=	Depth of Discharge
PEM	=	Proton Exchange Membrane
MGCC	=	MicroGrid Central Controller
EL	=	Electrolyser
FC	=	Fuel Cell
CRM	=	Capacity Reserve Margin
LLU	=	Loss of Largest Unit
HLI	=	Hierarchy level I
HLII	=	Hierarchy level II
HLIII	=	Hierarchy level III
MMTF	=	Mean Time To Failure
MTTR	=	Mean Time To Repair
FOR	=	Forced Outage Rate
COPT	=	Capacity Outage Probability Table
A	=	Available
U	=	Unavailable
D	=	Derated state
LOLP	=	Loss Of Load Probability
LOLE	=	Loss Of Load Expectation
EENS	=	Expected Energy Not Supplied
LOEE	=	Loss Of Energy Expectation
MCS	=	Monte Carlo Simulations
TTF	=	Time To Failure
TTR	=	Time To Repair

Chapter 1

Introduction

1.1 Background and objective

The network companies in Norway are obliged by law to provide grid connection to costumers in their region, only with a few exceptions. The country is sparsely populated. Nevertheless, people have populated some of the numerous remote islands along the long coastline. Today the power supply to these islands is secured through submarine cables or by installing diesel generators. While sub-marine cables pose as a costly alternative, the diesel generators contribute to CO_2-emissions. Hence, the network companies are looking for other solutions to ensure access to electricity in these areas.

As a part of an EU-funded project, TrønderEnergi is currently researching the possibility of implementing microgrid configurations containing renewable power sources at remote islands. At a test site at Rye outside Trondheim, a microgrid consisting of a wind turbine, a PV-system, a battery energy storage system and a hydrogen energy storage system has been installed. The grid will by the summer of 2020 be set in autonomous operation and provide power to the farm Langørgen Øvre. The microgrid will work as a technical pilot and is also equipped with a diesel generator as a backup solution.

To ensure secure and reliable operation of the microgrid a master-slave control strategy has been implemented to administer the operation of the resources. In this strategy, the battery is used as the master unit, responsible for maintaining the desired frequency and voltage level in the microgrid.

The choice of control logic will highly affect the operation of the microgrid, and the objective of this thesis is to investigate how different choices of control strategy influence the reliability performance of the microgrid at Rye. Four cases, each with a different control strategy, will be developed and investigated by means of reliability theory. The cases are

as follows:

- Case 1 - The control strategy already implemented at Rye. A master-slave control strategy with the battery as master-unit.
- Case 2 - A master-slave control strategy with the battery as master-unit and demand-side management.
- Case 3 - A master-slave control strategy with both the battery and the hydrogen system as master-units.
- Case 4 - A peer-to-peer control strategy.

A model of the microgrid will be obtained for each of the cases. Three adequacy indices, LOLP, LOLE and EENS, will be calculated using both an analytical method and Monte Carlo Simulations. This will form the foundation of the comparison of the performance of the four control strategies.

1.2 Report outline

The structure of this report aims to give a technical overview of the microgrid at Rye, relevant control system theory and a presentation of the cases examined. Additionally, an introduction to reliability theory and the methodology used to perform adequacy assessments will be presented.

Chapter 2 - *Rye microgrid*, provides a technical overview of the microgrid at Rye.

Chapter 3 - *Control strategies and degradation of hydrogen system components*, contains theory about two control strategies commonly used in microgrids and information about how the degradation of fuel cells and electrolysers are affected by the way they are operated.

Chapter 4 - *Cases*, presents the control strategies in the four cases.

Chapter 5 - *Power system reliability*, gives a brief introduction to power system reliability.

Chapter 6 - *HLI- and HLII Probabilistic Adequacy Assessment*, provides theory about the analytical method and Monte Carlo Simulations, both of which are used to analyse the adequacy of the four cases.

Chapter 7 - *Methodology*, presents the methodology used when modelling the operation of the microgrid in the four cases and performing the adequacy analysis.

Chapter 8 - *Results*, constitutes of the results acquired in the adequacy assessments.

Chapter 9 - *Discussion*, provides an analysis of the results acquired and a discussion of how the control strategies affect the adequacy performance of the microgrid.

Chapter 10 - *Conclusion*, summarises the main findings of the study.

1.3 Relation with the Specialisation Project

This thesis is a continuation of the specialisation project delivered in the subject TET4520 and written for NTNU in the fall of 2019, [19]. The theme of this thesis overlaps with that presented in the specialisation project. Parts of the theory, background information and methods presented in the project that is relevant for this thesis will, thereby, be reused. This applies to the following chapters:

- Chapter 2 - Rye microgrid
- Section 4.1 - Case 1 - The original system
- Chapter 5 - Power system reliability
- Section 6.1 - An analytical method for HLI adequacy assessment
- Section 6.2.2 - Probabilistic indices

Chapter 2

Rye microgrid

2.1 The REMOTE project

The microgrid at Rye is one of four demonstrations in the EU-funded project REMOTE (Remote area Energy supply with Multiple Options for integrated hydrogen-based TEchnologies). This project is a four-year project as a part of the Horizon 2020 program. Horizon 2020 is an EU initiated research and innovation program created to support and inspire scientific development and discoveries to ensure Europe's global competitiveness [20].

The REMOTE-project contains four demonstration sights where isolated microgrid configurations are installed in remote areas to supply inhabitants with renewable energy. The home page of the project states that: "[The project is] aimed to demonstrate the technical and economic feasibility of [...] fuel cells-based H2 energy storage solutions." [7]. The microgrids are located in the south of Italy, demo 1, Greece, demo 2, north of Italy, demo 3, and Norway, demo 4. Fig. 2.1 depicts an overview of the four demonstration sights and the power sources utilised at different locations.

The location of the microgrid pilot in Norway was initially intended to be Froan Island, located on the cost outside Trondheim. Due to protected wildlife on the island, the process to get concession is demanding and tedious. The microgrid was, therefore, moved to Rye, a small village on the mainland 12 km outside Trondheim. The objective of the project is to test the viability of the microgrid. The results will be used to assemble a similar microgrid at Froan, or other remote islands, at a later time. Froan presents a tougher climate than Rye, and measures to prevent corrosion and damage by strong wind gusts must be conducted when the microgrid is placed on Froan.

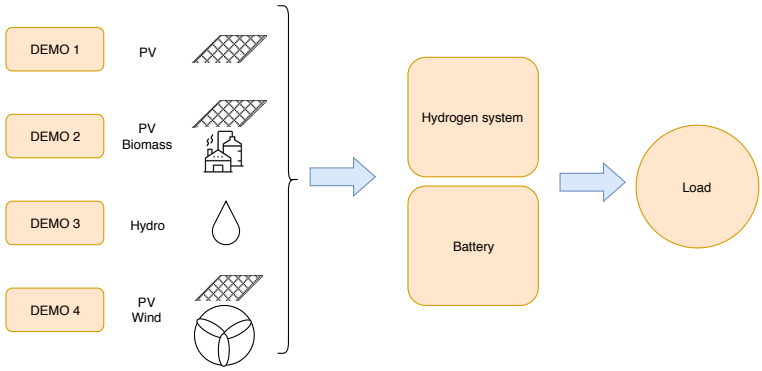

Figure 2.1: Overview of renewable energy sources utilised in the demonstration sights in the REMOTE-project [7].

2.2 Technical description

The microgrid at Rye consists of two renewable energy generating units: a wind turbine and solar panels. These are mature technologies that are well suited to supply the grid with energy. However, these sources are fluctuating and therefore balancing units for energy storage are needed. There are two energy storage devices: a battery and a hydrogen plant (electrolyser, hydrogen tank and fuel cell). Besides this, there is also a farm load, multiple converters, transformers and a backup diesel generator. In fig. 2.2, a general overview of the system in question is shown, its components and their connection. Some components, like circuit breakers, earth connections and measurement devices, are not included in the figure.

The microgrid will provide power to the farm Langørgen Øvre, and in the project a target value of availability greater than 98% was set with the given configuration [21].

2.2.1 Photovoltaic system

The generation of power from the sun at Rye is done by PhotoVoltaic (PV) modules mounted on the ground. To have a functioning PV-plant several components are necessary. The main components of the installation are the PV-modules, power optimisers, inverters and a control unit, as well as measuring devices for irradiation and temperature. Some of the components used in the PV-system at Rye, their type specification and unit numbers are listed in table 2.1. Other components needed are cabling, mounting system and weather protection.[1]

The system is built up as pictured in fig. 2.3. The panels are connected in 9 strings of 32 panels. For every second panel, there is a power optimiser connected, to ensure efficient operation, which will later be described in more detail. The panels are then connected to

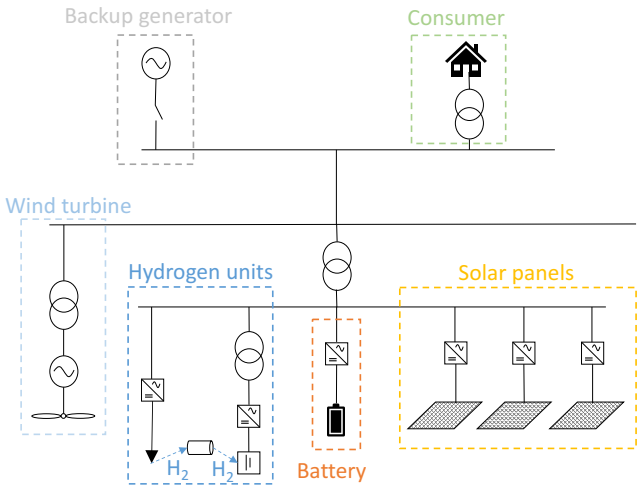

Figure 2.2: Overview of the Microgrid at Rye including the energy sources and storage units. Technical components, such as circuit breakers and earth connections, are excluded.

Table 2.1: Components of the PV-system at Rye [1].

Component	Type	Number of units
PV module	REC TwinPeak2 310 Wp	104
PV module	REC TwinPeak2 295 Wp	184
Inverter	SolarEdge 27.6K	3
Power Optimiser	SolarEdge P600	92
Power Optimiser	SolarEdge P650	52

three inverters which ensure AC at the microgrid connection. The PV-system was installed in the spring of 2019 and production went live on 8 April 2019. The production has since then been measured every 15 minutes.

The system will have a total installed capacity of 86.4 kWp. Through simulations by SolarEdge, this is expected to result in a maximum AC power of 82.8 kW out of the inverter [22].

Since the PV-panels were installed and put in operation, the generated energy has been measured. The monthly generated energy from the PV-plant is given in fig. 2.4. It must be noted that the recorded measurements from January-April are from 2020, while the remaining months were recorded in 2019. This plot will not represent each year, as there are variations.

All PV-modules have an I-V-curve, a relation between the current and voltage out of the solar panel. As power is the product of current and voltage, there is a point on this curve which gives the maximum power output: known as the Maximum Power Point (MPP)

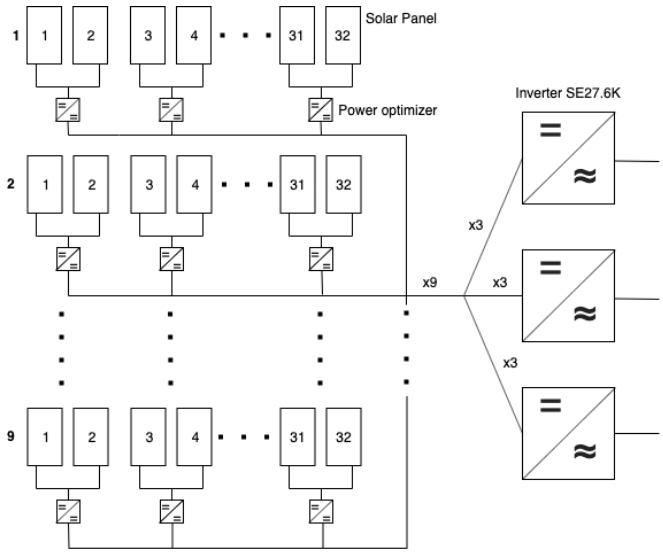

Figure 2.3: Construction of the PV-system at Rye, including panels (1-32 per string, 9 strings), power optimizers (one for every second panel) and inverters, with inspiration from [8].

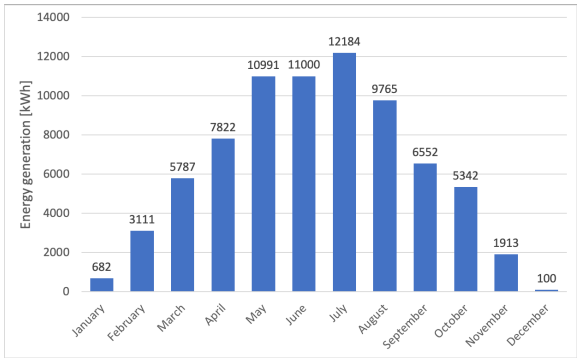

Figure 2.4: The measured energy generation from solar panels at Rye. Measurements from January-April are collected in 2020, while measurements from May-December are collected in 2019.

[23]. The solar installations are equipped with ”power optimisers” or ”Maximum Power Point Trackers” (MPPT) to ensure production at the MPP. The MPPTs are essentially DC/DC converters in which the duty cycle is adapted by control systems that monitor the performance of each module and adapts the voltage such that they are operated at the MPP. Another advantage of installing the power optimisers is that they measure the performance of each module, enabling efficient maintenance at module level [23].

To exchange power between the photovoltaic system and the grid an inverter is needed. The modules produce a direct current which must be converted to AC before delivered

to the grid. Three three-phase inverters, SolarEdge27.6k, are utilised in the PV-system at Rye. This inverter has an efficiency of 98% and a 12 years warranty. Each of the inverters is connected as depicted in fig. 2.3. [24]

Based on the setpoints of active and reactive power, the local controller assures the desired power transmission from the inverter. The three SolarEdge27.6k inverters have a rated output of 27600 VA, giving a maximum transmitting level of 82.8 kVA. This is lower than the installed capacity of the PV-system, which is 86.4 kWp. The maximum transmitting level of the inverter is hence the limiting element during optimal PV operation.

2.2.2 Wind system

Collection of the energy in the wind is done by a wind turbine of the type Vestas V27 [25]. It was bought second hand from Denmark by the owner of the land and installed in 2015. The power curve of the turbine in question is given in fig. 2.5, with a cut-in wind speed of 3.5 m/s, a rated wind speed of 14 m/s and a cut-off wind speed of 25 m/s. The turbine has a survival wind speed of 56 m/s [2].

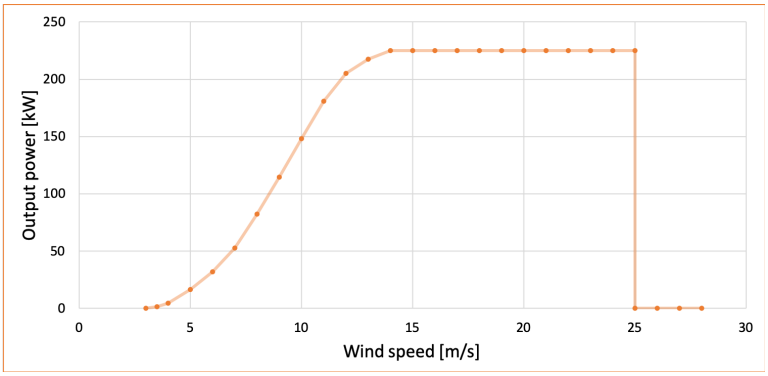

Figure 2.5: Power curve of the wind turbine VESTAS V27 [2].

Three rotor blades are assembled on a pitch regulated rotor. The turbine is upwind and has active yaw motors. From the rotor, the power is transmitted through a shaft and a two-stage gearbox to the generator. The generator has two sets of windings and can, therefore, operate both as a 6- or an 8-pole generator. This is to ensure optimal operation of the generator at different wind speeds. Consequently, there are also different ratings for speed, power and current.

The generator connected to the wind turbine is an asynchronous generator. In an asynchronous generator excitation current is required to produce a magnetisation flux which will induce rotor current. To provide magnetisation of the machine the generator will draw reactive power from the grid of which it is connected. The reactive power consumption is considerable, and a capacitor bank is often installed in parallel with the generator to

provide reactive power and adjust the power factor of the machine. Consequently, capacitor compensation is installed at Rye. The resulting power factor of the wind generation unit varies between 1 and 0.98 [26]. An approximation of the PQ-characteristics after the capacitor compensation can be seen in fig. 2.6

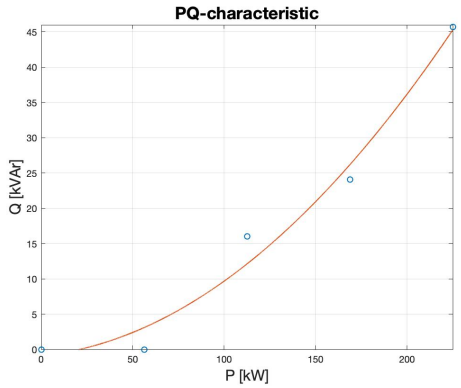

Figure 2.6: An approximation of the active power-reactive power characteristic of the asynchronous generator after capacitor bank compensation.

The generator is directly connected to the rest of the grid through a transformer. Some of the main sizes of the wind turbine are given in table 2.2 while the detailed information can be found in [2].

Table 2.2: Important sizes of the wind turbine at Rye[2]

Type specification	VESTAS V27, 50Hz tubular tower
Hub height	31.5 m
Rotor diameter	27 m
Generator rated power	225 kW
Generator rated voltage	400 V

The wind turbine has been operative for several years. An improvement of the operation and control of the system and the pitch control system in 2017, have however increased the generation level [25]. The generation on a monthly basis of the past year may be found in fig. 2.7.

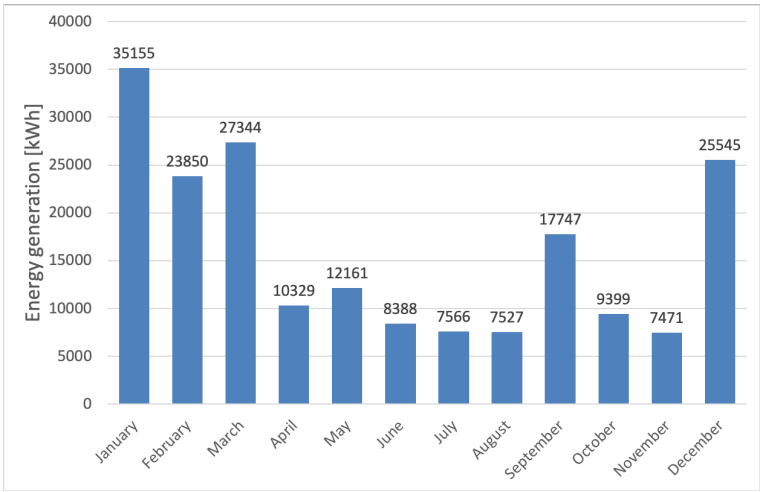

Figure 2.7: Measured energy production from the wind turbine at Rye. January-April is measured in 2020, while May-December were measured in 2019.

2.2.3 Energy storage

As previously mentioned, an Energy Storage System (ESS) is necessary to balance the fluctuating sources in the system. The system contains two main storage units, a Battery Energy Storage System (BESS) and a Hydrogen Energy Storage System (HESS). The battery and the hydrogen unit have a storage capacity of 554 kWh and 1.67 MWh, respectively [9]. These two storage technologies are well known, and their area of application will complement each other well in a microgrid configuration. The BESS provides fast-acting energy storage, while the HESS has a higher response time. The HESS has, however, a higher energy density and larger storage capacity than the BESS.

Battery Energy Storage System

The battery used in the BESS is a lithium-ion battery with a capacity of 554 kWh, a maximum apparent power of 400 kVA and efficiency of 98% [27]. The BESS does not only consist of a battery; it is a composite system of several components, such as a power conversion system, a local control unit and protection units, in addition to the battery. As power will flow both from and to the BESS, the storage system requires a bidirectional converter. The converter utilised in the BESS at Rye has an efficiency of 98% and a rated current of 540 A [9].

The battery is produced by LG Chem, one of the worlds largest manufacturers of lithium-ion batteries. The battery in the BESS at Rye contains 85 modules with an energy capacity of 6.67 kWh each [9]. These modules are connected in series of 17, constituting five

racks. Each rack has a capacity of 113.5 kWh, and they are connected in parallel, giving the BESS a total capacity of 554kWh. The configuration of the battery system can be seen in fig. 2.8.

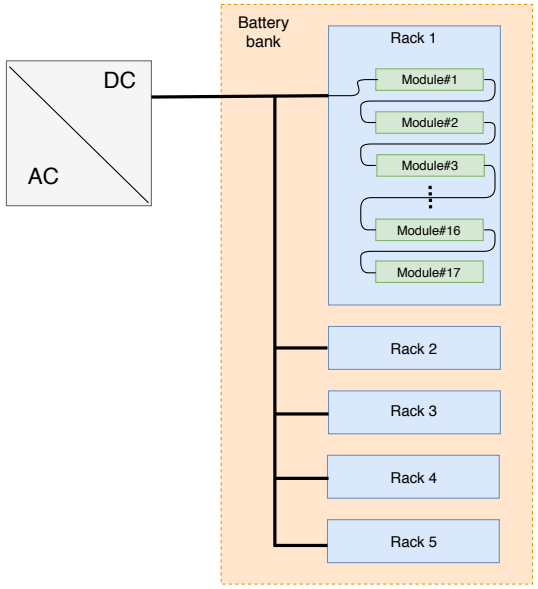

Figure 2.8: Illustration of the configuration used in the LG Chem battery used at Rye.

The performance of the batteries is assumed to be highly dependent on the State of Charge (SoC) and Depth of Discharge (DoD). SoC is the percentage of energy stored in the battery at a given time, while the DoD indicates the percentage of energy already drawn from the battery. The battery used in the microgrid at Rye has a lifetime of approximately ten years, considering 400 complete cycles per year [9]. One cycle represents a complete discharge of the battery, from SoC 100% to 0%. Batteries experience a decrease in lifetime cycles with an increasing DoD [28]. Lithium-ion batteries are recommended to run at an SoC between 20 and 90% (equivalent to a DoD in the range 10-80%). In this range, the number of lifetime cycles will be upheld, while one still can utilise a significant percentage of the battery capacity. This increases the usable capacity of the battery without decreasing the lifetime.

The DoD at which the battery is operated will also affect the efficiency. Fig. 2.9 shows the charge- and discharge limits for the battery used at Rye. The battery is capable of high discharge rates within given limits, ensuring high efficiency during times of vast power exchange with the grid. At an SoC close to 0% and 100% the discharge- and charge rate decreases drastically. To avoid a scenario where the BESS is incapable of safeguarding the frequency- and voltage level, the control system must strive to avoid these levels of SoC of the battery.

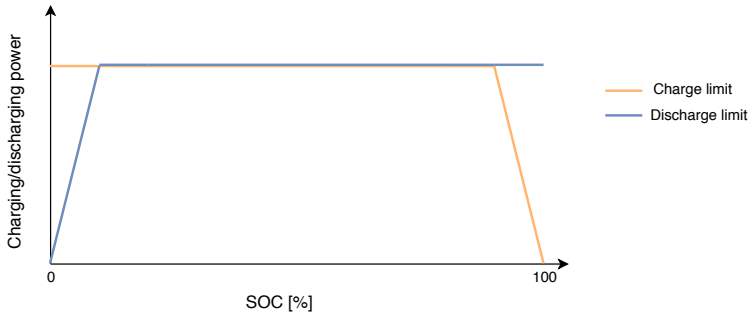

Figure 2.9: Battery charge/discharge limits, inspired by information in [9]

Hydrogen Energy Storage System

The HESS consists of an electrolyser with a rectifier, a hydrogen storage unit, a fuel cell with an inverter, as well as temperature regulating equipment and control- and protection units. At Rye, the electrolyser is delivered by Hydrogenics, while Ballard is responsible for the fuel cell. The storage can hold 100 kg H_2 at a pressure of 30 bar. This is equivalent to approximately 1.67 MWh output of the fuel cell [9].

Electrolyser

The electrolyser utilises electric energy to produce hydrogen. The unit is connected to a rectifier which transfers a DC voltage of 400 V [9]. The nominal input of the electrolyser is 55 kW. The electrolyser at Rye is a Proton Exchange Membrane (PEM) electrolysis cell. The red-ox reaction that takes place during hydrogen production is as follows [29]:

$$Anode : H_2O \rightarrow \frac{1}{2}O_2 + 2H^+ + 2e^-$$

$$Cathode : 2H^+ + 2e^- \rightarrow H_2$$

The efficiency of the PEM electrolyser can be seen in fig. 2.10. As can be seen, the efficiency peaks at a power approximately around 20% of nominal power, and decreases at higher power levels. Additionally, the efficiency will decrease drastically at lower power ratings.

H_2-container

In the system at Rye, the produced H_2-gas gets pressurised before stored in a hydrogen container. The container can hold 100 kg H_2 at a maximum pressure of 30 bar. Hydrogen

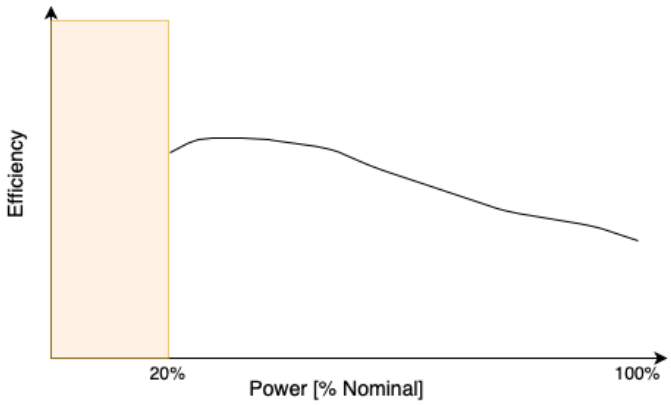

Figure 2.10: Electrolyzer efficiency vs. power (% of nominal), inspired by graph in [9].

has an energy density of approximately 33.33 kWh/kg [29], and the container can, therefore, store a maximum of ca. 3.3 MWh. As the fuel cell efficiency can be approximated to just above 50 %, the amount of usable energy is roughly 1.67 MWh [9].

Fuel cell

In cases of energy shortage in the microgrid, hydrogen is converted to electric energy through a fuel cell. The fuel cell will reverse the reaction in the electrolyser. The PEM fuel cell is a 100 kW source which delivers a voltage to an inverter. The inverter is further connected to a transformer which transforms the now alternating voltage to a level of 400 V.

The variations in the efficiency of this PEM fuel cell, according to the power supply, can be seen in fig. 2.11. One strives to operate the fuel cell in the marked area of the figure, where the efficiency peaks.

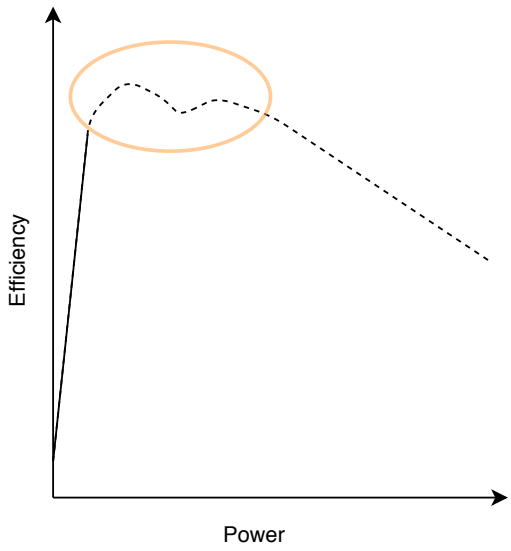

Figure 2.11: Fuel cell efficiency vs. power, inspired by graph in [9].

2.2.4 Load

The farm Langørgen Øvre will serve as the load in this microgrid. The farm consists of three buildings: a residential house and two barns. When designing the microgrid, the annual consumption was measured to be 126.75 MWh [25]. However, an increase in the consumption level has been detected the last year, increasing the annual consumption to 176 MWh. The variations in load throughout a year can be seen in fig. 2.12.

The consumption profile varies with the seasons, and the average load is higher during the winter. It can be seen from the load profile that the peak load is 72.45 kW. Power-intensive equipment, such as equipment used in the grain drying process and milking robots, causes periods of high consumption at the farm.

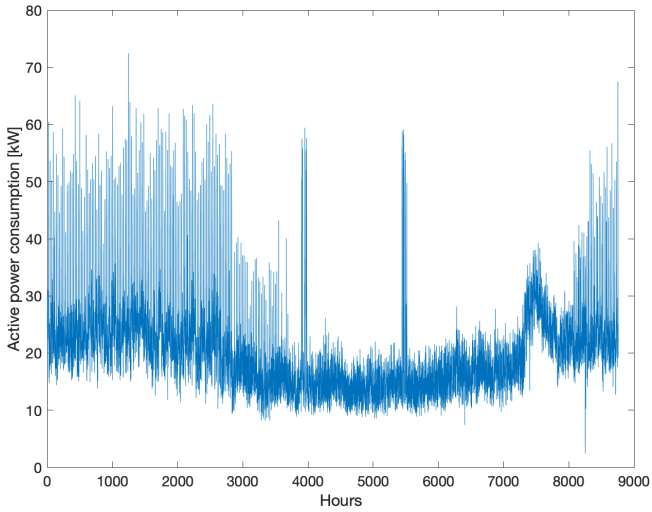

Figure 2.12: Load profile of Rye microgrid. The graph is made out of consumption measurements throughout a year recorded from the end of April 2019 to the end of April 2020.

2.2.5 Backup system

A diesel generator will be utilised as a backup for the microgrid in case of near energy shortage. This is a 66 kVA synchronous generator [30]. Before connecting the diesel generator, it must be synchronised with the grid. This is to avoid opposite power flow and damage of the generator.

A diesel generator is only one of several options for backup systems. Microgrids located close to the utility grid can utilise a direct connection to the grid as a backup. An extension of the HESS can also be an alternative. By providing the system with a hydrogen depot and an extra fuel cell, this can provide the system with backup power. For the microgrid at Rye, the diesel generator was considered a more robust option.

Chapter 3

Control strategies and degradation of hydrogen system components

3.1 Control strategies

A microgrid consists of a collection of micro-sources operated together. The grid can be operated either as a synchronised part of the utility grid or in autonomous mode, as an individual unit. Usually, when the microgrid is connected to the main grid, the utility will be responsible for frequency and voltage control. Hence, the sources within the microgrid will inject or absorb power following given setpoints. This type of control is called power control. Whenever the microgrid is operating in island-mode, the frequency and voltage control must be maintained by the microgrid itself, and a control strategy is needed. Numerous different control strategies exist, but two of the most common strategies used in microgrids are called master-slave and peer-to-peer [31]. Although these strategies are used separately in many configurations, a combination of the two is common. In the following paragraphs, the two strategies will be further explained.

3.1.1 Master-slave strategy

As the name suggests, the master-slave strategy divides the resources in the microgrid into two groups: masters and slaves [31]. One or more of the units acts as masters, while the rest of the units acts as slaves. A master controller is also present, giving the units setpoints of operation. When this control strategy is utilised, the sources will be power controlled

during grid operations. During these conditions, the utility grid will be responsible for frequency and voltage control, and the units within the microgrid will be governed based on setpoints of active and reactive power. During island operation, the units categorised as slaves will continue their operation in power control mode, acting on setpoints given by the master controller. The function of the master unit will, however, change when the microgrid switches to autonomous mode. During this mode, the master will be responsible for the frequency and voltage control in the microgrid. The master is provided with setpoints of the desired voltage and frequency by the master controller. Based on these setpoints, along with measurements of the state in the system, the controls of the master units adjust the amount of active and reactive power needed to be injected or absorbed in the system to obtain the given frequency and voltage levels.

A communication system is required for the master controller to exchange setpoints with the resources. Communication is also needed to provide the master controller with states and conditions of the units. In a microgrid containing renewable energy sources, the aim of the master controller will often be to harness as much of the available energy as possible. The setpoints provided for the slave units will thereby vary based on available energy and load fluctuations. The master will then be responsible for ensuring power balance and stability in the system.

Figure 3.1 depicts the master-slave control scheme. In the figure, it can be observed that the master controller, denoted as MicroGrid Central Controller (MGCC), provides the slave unit on the right-hand side with settings of P and Q. These settings are supplied to the local controller, which distributes the settings to the prime mover and the PQ control of the converter. This way, the local controller assures the correct production level of P and Q from the given slave unit. On the left-hand side, the MGCC provides the local controller of the master unit with setpoints of V and f. The master unit will then strive to maintain the given voltage and frequency level. Employing secondary control, the master controller can assure a fixed voltage level and zero frequency deviation [10]. This is a definite advantage.

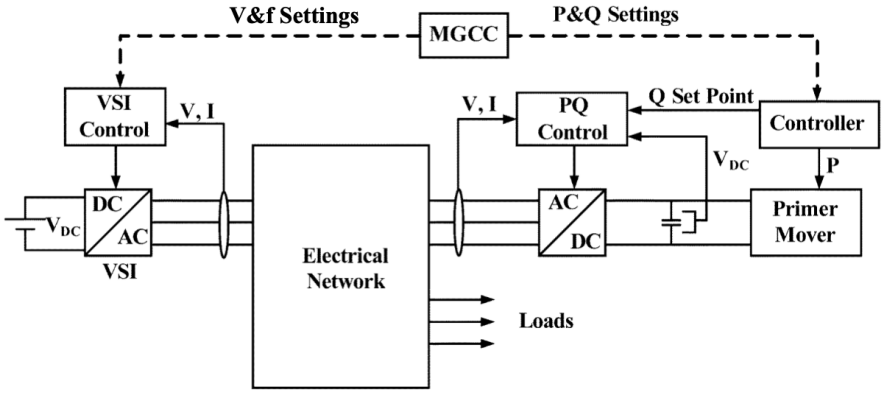

Figure 3.1: Illustration of a typical master-slave control scheme [10].

The master-slave strategy does, however, have a couple of downsides. The microgrid is sensitive to faults in the master unit, master controller and communication system. Faults and unavailability in these parts of the system may cause the whole system to break down [31, 11, 32]. This is one of the reasons why the master-slave strategy is primarily used in small microgrids. Furthermore, advanced detection and control of transformation from grid connection mode to island mode is needed [31]. The function of the master units must switch from power controlled to frequency and voltage-controlled within a time frame of milliseconds. Thus, a well-operated switching scheme is fundamental.

3.1.2 Peer-to-peer strategy

Unlike in the master-slave strategy, all the resources will have the same functions when utilising a peer-to-peer strategy. The units in the microgrid will, in both in grid-connected mode and island mode, contribute to both voltage and frequency regulation. This is done by means of droop control. Droop control is a conventional way to regulate power plants with synchronous generators, even though the principle can be used for any generation unit [33].

When utilising the droop control strategy, the frequency is used as an indicator of the power balance of the system. This is due to the relation between the power balance and frequency in a rotating machine, given by the swing equation in eq. (3.1).

$$\frac{2H}{\omega_s}\frac{d^2\delta}{dt^2} = P_m - P_e - P_d = P_{acc} \tag{3.1}$$

H is the inertia constant, ω_s is the angular speed, and δ denotes the power angle. Additionally, P_m, P_e, P_d and P_{acc} denotes the mechanical, electrical, damping and acceleration power, respectively.

A change in frequency, and thereby a change in power angle, will cause an unbalance and a change in power output of the generator, as can be seen from eq. (3.1). A decrease in frequency will cause the machine to accelerate, and an increase in frequency will cause the machine to decelerate. The inertia of the rotating machine causes an automatic response to the frequency change. This characteristic is taken advantage of in the peer-to-peer control strategy.

Microgrids consisting mostly of power electronics and few rotating machines are low inertia systems. The principle of the rotating machines can, however, be imitated. The power electronics can be controlled to act as rotating machines, adopting the characteristics. This allows for a peer-to-peer strategy based on droop control in low inertia systems too.

Using this strategy a change in load or excess energy in the system will be distributed among the sources in accordance with the droop factor. Assuming $X \gg R$, a small power angle δ and small variations in voltage level in the system, the frequency depends

predominantly on the active power, P, while changes in voltage depend predominantly on the reactive power, Q [12, 33, 34]. Eq. (3.2) and (3.3) show the dependencies and how the units will react to changes in the system following the droop, k_p and k_q [12].

$$f - f_0 = -k_p(P - P_0) \tag{3.2}$$

$$U_1 - U_0 = -k_q(Q - Q_0) \tag{3.3}$$

In the equations f_0 and U_0 are rated frequency and voltage, P_0 and Q_0 are the momentary setpoints for active and reactive power and f, U_1, P and Q are the actual values in the system at the given time. An example of the droop characteristics of two micro sources and a storage unit is given in fig. 3.3.

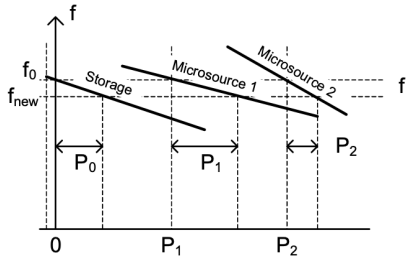

(a) Illustration of frequency control during droop control.

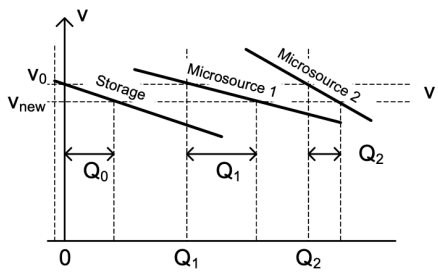

(b) Illustration of voltage control during droop control.

Figure 3.2: Droop characteristics [11].

If the assumption of $X \gg R$ is invalid eq. (3.4) and (3.5) must be used [12].

$$f - f_0 = -k_p \frac{X}{Z}(P - P_0) + k_p \frac{R}{Z}(Q - Q_0) \tag{3.4}$$

$$U_1 - U_0 = -k_q \frac{R}{Z}(P - P_0) - k_q \frac{X}{Z}(Q - Q_0) \tag{3.5}$$

Fig. fig. 3.3 depicts how the line impedance ratio affects the droop characteristics. As can be seen, a pure resistive line will result in reverse droop control. Hence, a change in reactive power will impact the frequency, while a change in active power will affect the voltage level.

When using the peer-to-peer control strategy, no superior control system, nor critical communication between the units are needed [32]. Each of the resources in the microgrid will contribute to restoring the desired frequency and voltage level when fluctuations are detected. This calls for a more reliable system, as the operation of the microgrid is possible despite failure or unavailability of one or several units. A steady-state error in frequency and voltage will, however, appear if no secondary control mechanisms are implemented

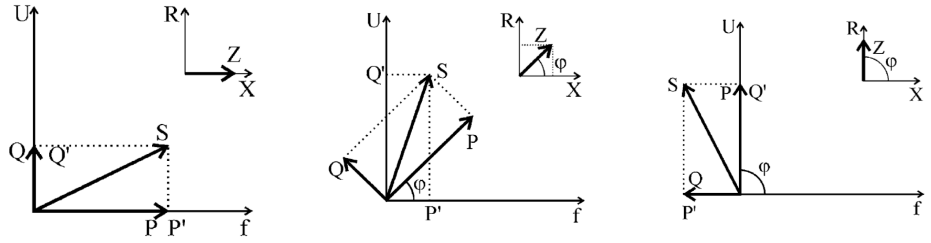

(a) R/X = 0.

(b) R/X = 1.

(c) R/X = ∞.

Figure 3.3: Impact of line impedance ratio on the droop characteristic [12].

[31]. Additionally, the droop control can prevent full utilisation of the renewable sources and suboptimal distribution of spinning reserves. This is because the generation units are adjusted in line with the load condition and not the renewable energy resources available [32].

3.2 Degrading of electrolysers and fuel cells

The choice of control strategy will have a considerable impact on how the components in the microgrid are operated. The operation of the components is especially important when investigating the performance and reliability of the hydrogen storage units.

Both the electrolyser and fuel cell at Rye utilise PEM technology. These components consist of few mechanical parts, resulting in high availability, due to few parts in which can cause failure [35]. Degradation is, on the other hand, common among these components. The efficiency of the chemical processes within the components degrades with time due to, among other things, corrosion of the catalyst and membrane degradation [36, 37]. As a result, the internal resistance increases, and there will be a decline in performance. Furthermore, the fuel cell voltage decreases [37].

The speed of the ageing of the hydrogen system is highly dependent on the way it is operated. It can be seen that the life span of electrolysers and fuel cells decreases whenever the units are forced to perform stop and start-procedures [37, 38, 39]. It has also been found that the accelerated ageing of the fuel cells correlates with operation in load-following mode, where the power generated of the fuel cell varies [13]. The impact of start and stop-operation and load changing on fuel cell degradation is depicted in fig. 3.4. The degradation can be considerably decelerated by minimising these operation modes.

It is reasonable to believe that similar degradation patterns can be found for electrolysers during discontinuous operation, but this has not been confirmed [38]. However, the electrolysers are sensitive to high current densities, which can cause faster degradation.

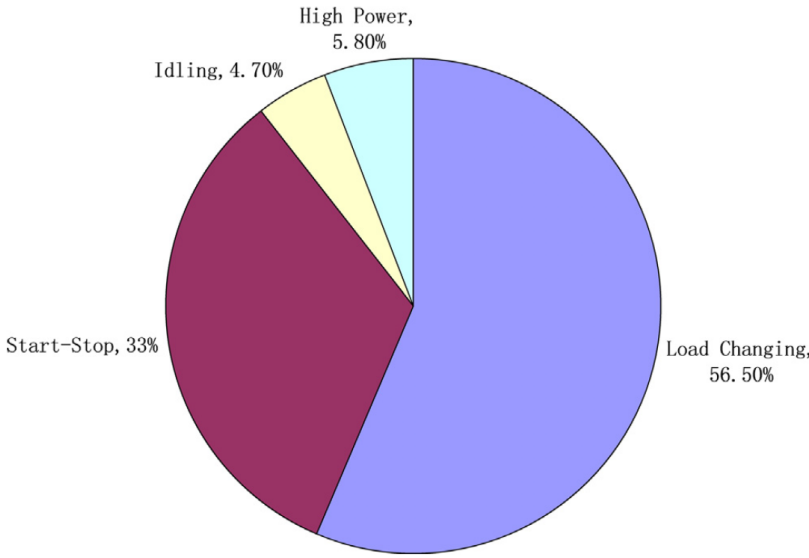

Figure 3.4: Degradation rates due to different operation conditions [13].

Chapter 4

Cases

In this section, four cases utilising four different control strategies will be presented. These cases will form the basis of the reliability assessments performed in the thesis. First, the original control scheme will be presented. This is the control strategy implemented in the microgrid at Rye and utilises a master-slave strategy. Second, a slightly different master-slave control scheme will be presented. This system differs from the first case, as an opportunity for demand-side management is included.

Further, a third master-slave strategy will be presented. In this case, both the battery storage system and the hydrogen system will serve as masters. One can argue that the presence of two masters will improve the reliability of the system. Finally, the fourth case will be presented. In this case, the peer-to-peer control strategy will be utilised.

4.1 Case 1 - The original system

A master-slave control scheme is used in the microgrid at Rye. In this strategy, the master controller makes out the heart of the control system. This unit receives measurements from the resources, loads and storage units and decides how the energy generation and consumption of the grid should be distributed. This is, as explained in chapter 3, done by distributing V and f setpoints to master units and P and Q setpoints to slave units.

The BESS will serve the role as master in the microgrid at Rye. It has a fast response time and is, to a great extent, able to cancel out fluctuations and preserve the frequency at 50 Hz and the voltage at an acceptable level by balancing the active and reactive power in the system. The other units, the PV-system, the wind turbine and the hydrogen system will, thereby, operate as slaves in this control scheme.

The master controller coordinates the operation of the resources in the microgrid. However, the master controller at Rye has a rather large time step. Consequently, its task is not to manage dynamic responses or other fast phenomena. Its main objective in the microgrid is to manage energy generation and consumption in all components and for the system as a whole. The generation and consumption must be balanced at all times, but the fluctuating nature of both resources and load makes this a continuous challenge [40]. This should be performed simultaneously as the exploitation of the renewable sources should be maximised and minimising the use of the backup generator. Hence, the P and Q setpoints of the renewable sources are to any lengths possible set to the maximum amount possible.

At all components, there is a local control system which receives an order from the master controller and interacts with the component. It receives a setpoint at which it should stay, be it active and reactive power or voltage and frequency. Then, depending on the component in question alters the operating environment such that the component delivers what is asked. The local controllers also focus on the more dynamic responses and any control logic that requires a faster response, such as current control.

The communication between the components is performed with the protocol Modbus, which is a protocol for master/-slave communication of automated systems. Modbus is widely used in industry and enables communication between the different systems from different suppliers [41].

4.1.1 Control of the HESS

The logic surrounding activation and stopping of the components in the HESS is primarily built around the SoC of the battery. An overview of the logic can be seen in fig. 4.1.

As mentioned in section 2.2.3, it is desirable to limit the charging of the battery before it is fully charged. Therefore, if the renewable production is higher than the load and the battery is almost full, the master controller will activate the electrolyser. As can be seen in fig. 4.1, the electrolyser will be initiated at a given SoC of the BESS.

Due to drastically decreasing efficiency during operation at low power levels, the electrolyser is not operated at power levels below 20% of nominal power [9]. This is to ensure the optimal utilisation of surplus energy in the system. The number start and stop-cycles of the electrolyser highly influence the degradation and lifetime of the unit. The system will, thus, favour operation over more prolonged periods compared to frequent starts, to secure ideal operation. Therefore, in cases where the operation of the electrolyser is initiated, but the amount of surplus energy decreases below 20% of P_n, the battery will provide the electrolyser with power for a small period, awaiting a higher production from the generating sources. This is in principle, undesirable as energy is lost in all the conversions, but beneficial since it prevents short cycles of operation.

When the SoC of the battery comes under a certain threshold, the electrolyser is stopped. The electrolyser will, thus, operate within a certain range of BESS SoC.

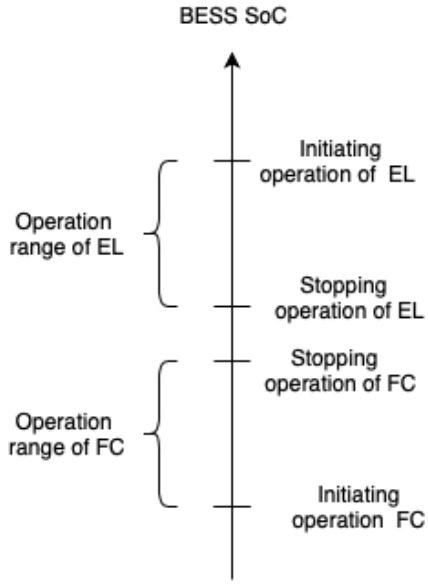

Figure 4.1: Conceptual overview of control of the HESS. SoC denotes the SoC-level of the BESS, EL denotes electrolyser and FC denotes the fuel cell.

If the SoC of the battery goes below a different threshold, the fuel cell operation is initiated. It may then supply the load with the missing power and contribute to recharge the battery.

During operating of the fuel cell, the main objective is to meet the power requirement of the load and maintain energy balance in the microgrid. Nevertheless, if the load requirement is low, the fuel cell will still operate at a power level of maximum efficiency, c.f. fig. 2.11, contributing to the recharging of the BESS. Furthermore, this operation of the fuel cell will prevent fluctuations in power, avoiding unnecessary degradation. When a certain level of SoC in the BESS is reached, the operation of the fuel cell will be terminated, and the BESS will again be the only unit balancing the energy level in the system. The range of fuel cell operation can be seen in fig. 4.1.

4.1.2 Curtailment of renewable sources

Usually, it is desirable to produce the maximum amount of power from both the PV-panels and the wind turbine. However, if the ESS SoC is at its maximum while the generation is higher than the load; the final option is to curtail the generation. The PV-generation will be curtailed at its inverters first, as this is the easiest to implement. Thereafter, wind generation will be limited. Curtailing the wind leads to mechanical stress on the turbine. This will be avoided as far as possible.

4.1.3 Backup generator

The backup generator will be activated if the BESS reaches below a certain level of SoC and thereby replace the battery as the master in the system. Further, the battery will take on the role of a slave. This implies that the system, in reality, has two masters, but they will not operate as masters simultaneously. Moreover, the master controller will provide setpoints to the BESS enduring recharging of the storage whenever excess energy is available. The generator will be operated at near full power contributing to recharging the storage, while also controlling the frequency and voltage level.

4.2 Case 2 - Master-slave strategy with demand-side management available

The second case uses a master-slave strategy similar to the one presented in case 1. The only change is the supplement of active load management. Active load management, also called demand-side management, includes measures which improve the energy system at the consumption side [42]. Examples of active load management are using better materials to improve efficiency, utilising smart tariffs to influence consumption patterns and using direct control of consumption units, also called load management. The latter will be included in the control strategy for case 2.

In a microgrid essentially based on volatile renewable sources and limited energy storage capacity, load management can be utilised to cut consumption and avoid operation of the backup diesel generator. The load management at Rye must, though, be somewhat restricted. Firstly, the farm holds livestock; thus, power is essential for machines which ensure the welfare of the animals and proper operation of the farm. Secondly, electric loads which are vital for a comfortable standard of living at the farm will not be considered as a part of the load management.

An investigation of the possibility of implementing demand-side management in the microgrid at Rye was performed by NTNU-students in the spring of 2019. Based on conversations with the farmer, Lars Hoem, the loads in the grid were sorted into three categories: flexible loads, non-flexible loads and power-shiftable loads [3]. No load management could be performed on the non-flexible loads, while the flexible loads could be curtailed for a given period. Finally, the power-shiftable loads were loads which could be operated at lower power consumption. In table 4.1, the flexible and power-shiftable loads in Rye microgrid are listed. A more extensive list of loads at the farm site can be found in [3].

The findings in [3] were actively used when implementing the demand-side management in the control logic of case 2. The logic was implemented as follows: A strong dependency between the SoC of the BESS and load management was established. No load curtailment will be performed at SoC-levels above 25%. Whenever the SoC decreases below 25% curtailment of the silo, if operated at the time will be initiated. Load data from separate

Table 4.1: Overview of loads flexible and power-shiftable loads which are included in the given control strategy. The tables is based on information found in [3].

Electrical unit	Power rating [kW]	Energy consumption [kWh]	Type	Limit
Water heater x 3	2-3	2-3	Flexible	12 hrs
Dishwasher x 3	-	1.28	Flexible	24 hrs
Washing machine x 3	-	1.55	Flexible	24 hrs
Telenor station	1.9	1.9	Power-shiftable	100%
Lights	1.95	1.95	Power-shiftable	20%
Silo	44	22	Flexible	16 hrs

circuits will be used to detect the operation of the different load units at the farm. As stated in table 4.1, the silo is a 44 kW flexible load, which can be curtailed for 16 hours. Hence, operation of the silo will again be initiated whenever the SoC is above 30% or if the time-shift of the silo-operation exceeds 16 hours.

Telenor has rented an area at the farm where telecommunication equipment is placed and connected to the microgrid. The power consumption of these telecommunication units will be cut, in addition to the curtailment of the silo, if the SoC of the battery reaches below 20 %. Additionally, an SoC below 15% will cause curtail of the light to a level of 20% and time-shifting of water heaters, dishwashers and washing machines if the operation of these units is detected. An overview of load management at different SoCs can be seen in table 4.2.

Table 4.2: Overview of load management measured activated at different SoC-levels of the BESS.

SoC-level	**Load management**
25%	- Time-shifting of the silo
20%	- Time-shifting of the silo - Curtailment of power supply to Telenor-equipment
15%	- Time-shifting of the silo - Curtailment of power supply to Telenor-equipment - Adjusting power supply to light to 20% of maximum - Time-shifting water heaters, dishwashers and washing machines

4.3 Case 3 - Master-slave strategy with two masters

The third case also utilises a master-slave control strategy. Also this case is based on the control scheme in case 1. In contrast with the control strategy in case 1, two of the units in the microgrid will serve as masters in this system. Three master units can, thus, be counted when including the diesel generator. The main goal is to run the microgrid solely

on renewable energy, operation of the diesel generator is still considered a backup solution and the generator will, therefore, not be counted as one of the primary master units. The increase from one to two main master units will contribute to increased reliability, as the system now is less vulnerable to faults.

The two main master units are the BESS and the HESS. These will, however, not operate simultaneously, allowing only one unit to control the frequency and voltage level at the time. Both units will, though, be equipped with a voltage source converters and a local regulator, allowing both PQ- and Vf- operation based on setpoints given from the master controller.

During regular operation, the same control strategy as presented in case 1 will be utilised. The BESS will operate as the master of the system, and the hydrogen system will be power controlled, dependent on setpoints of active and reactive power given by the master controller. The HESS will, however, inherit the role as the master whenever the SoC level of the BESS is beneath a given limit. During this time, the lower power limit of operation of the electrolyser in the HESS must be removed. This is to equip the HESS with the abilities to regulate the voltage and frequency of the microgrid.

Throughout operation with the HESS as master, the master controller will strive to recharge the battery with any given excess energy in the system. The roles will thereby change back to the BESS as the master and the HESS as a slave if the SoC of the battery exceeds a predefined limit. Besides, the HESS will replace the BESS as master if the BESS is unavailable, for example, due to a fault in the inverter or the battery itself. In this instance, the excess energy will be used to produce hydrogen. Curtailment of the renewable sources might be necessary to maintain a balanced system if excess energy is available and the hydrogen tank is full.

The dynamic response during the transformation from one master to another has not been tested. Seamless transition between the states is assumed in this thesis.

Whenever the HESS operates as master, the system must be able to follow and respond to the load and production changes. Neither the fuel cell nor the electrolyser installed at Rye is designed for this kind of operation. Thus the HESS is not well suited to work as the master unit in the microgrid at the present time. The electrolyser will not be able to respond quickly enough to rapid changes. The fuel cell can, on the other hand, enter a load-following mode, where the response of the fuel cell will be satisfactory. The response time will, however, not be adequate when the fuel cell initially is in ideal mode. Then the response will be in the range of seconds, not fast enough to ensure stability in the system.

To overcome these challenges, a small battery will be installed in parallel with the fuel cell and the electrolyser. This type of battery is often called auxiliary energy storage [35]. The fuel cell, electrolyser and the small battery will be viewed as one unit in the analysis, causing considerable improvement of the ramp rate of the hydrogen system. Fig. 4.2 depicts the configuration used in this thesis. More advanced coupling mechanisms might also be possible, allowing the battery to utilise the converters of the electrolyser and fuel

cell, but these mechanisms call for more advanced control logic.

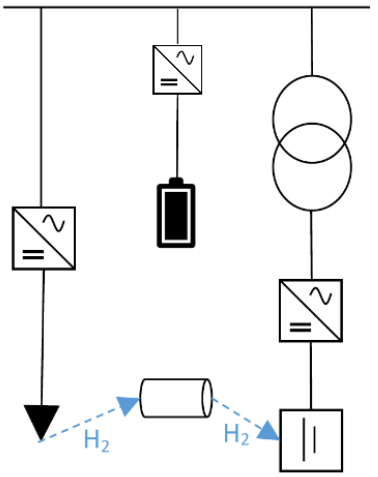

Figure 4.2: Configuration used to allow fast reaction to fluctuations in frequency and voltage in the microgrid. The battery is placed between the units in the HESS. It is charged when supporting the electrolyser and discharged when supporting the fuel cell.

The battery within the hydrogen system must have enough capacity to support the fuel cell during starts from ideal mode and the electrolyser whenever the power changes are too severe. A local control logic must be implemented to ensure correct charging and discharging of the auxiliary energy storage. The size of the storage unit is dependent on this logic and the performance of the fuel cell and electrolyser. This was not investigated in this thesis and must be further examined before one can conclude on optimal storage size. Nor was the dynamic performance of this hydrogen system examined. Tests of the dynamic response must, also, be performed to validate that the given configuration can be utilised. In this thesis, the assumption that the given system will work has been made.

The diesel generator will, in similarity with case 1, be utilised as the master in case of unavailability of both the BESS and the HESS. During operation of the backup generator, the master controller will strive to recharge the battery. The BESS will then be reinstated as master of the system when the SoC exceeds a predefined threshold.

In the case of unavailability of the BESS during operation of the diesel generator, the master controller will aim to recharge the HESS. The HESS will then take over the role as master when a given amount of hydrogen is produced.

4.4 Case 4 - Peer-to-peer strategy

In the last case, a peer-to-peer strategy will be utilised to control the microgrid. No communication system between the units will be necessary, as all the units contribute to frequency and voltage regulation employing droop control in the local controllers. The assumption of $X \gg R$ has been made, and the droop control will follow the characteristics stated in eq. (3.2) and eq. (3.3).

The same configuration as described in case 3, depicted in fig. 4.2, will be used for the hydrogen system. This allows the HESS to contribute in the same manner as the BESS, with rapid responses to fluctuations in frequency and voltage. To enable the HESS to contribute with frequency and voltage control at low power rating, the lower power limit of operation of the electrolyser must be removed, despite the decrease of efficiency.

Some modifications have, however, been implemented in the droop control of the renewable power sources. To avoid unnecessary curtailment the renewable resources are allowed to produce the maximum amount of available power. The droop control will, however, be initiated at a higher degree of over-frequency in the system. If the frequency exceeds 51 Hz, the droop control will be activated, and some of the power production will be curtailed.

Besides, modifications have been done with the local control of the backup generator too. The generator will only be initiated whenever the storage units are unavailable. During operation, the generation will be included in the peer-to-peer control strategy, and the power output will be determined by the droop of the machine and the frequency variations in the microgrid.

Tab. 4.3 lists the droop factors of the resources in the system used during simulations.

Table 4.3: Droop factors of different units in the microgrid at Rye used in simulations of case 4.

Unit	**Droop** [%]
Wind turbine	7
PV-system	7
BESS	4
HESS	4
Backup generator	4

Chapter 5

Power system reliability

The reliability of the power grid has always been an essential concern for power system planners. The grid consists of numerous components causing extreme complexity. To ensure reliable operation of the grid reliability criteria have been developed. These criteria are present to describe the amount of stress the grid can handle without compromising a stable operation. Historically the indices used for planning and operation were deterministic, and one of the most used criteria is the N-1 (or N-2) criteria. This criterion implies that the grid must be able to operate within acceptable operating limits despite the loss of any unit (or any two units), i.e. a line, a transformer or a generator [43]. In stand-alone power systems, such as island operated microgrids, other deterministic criteria, such as fixed Capacity Reserve Margins (CRM) or Loss of Largest Unit (LLU), have been common [17].

Deterministic reliability criteria are easy to interpret, but they do not consider the inherent uncertainty of failure of components or change in load demand. The uncertainty of production level of renewable sources, due to the dependency of weather conditions, is likewise not included in the deterministic reliability criteria. These uncertainties might have a considerable impact on the reliability performance of the grid. To account for the stochastic behaviour of the components probabilistic reliability indices have been developed. This chapter will present different aspects of reliability evaluation and introduce the theory behind some of the methods used when performing a reliability analysis of the microgrid at Rye.

5.1 Adequacy and security

In [44], the author presents two definitions of reliability:

1. The ability of an item to perform a required function under stated con-

ditions for a stated period of time.

2. The characteristic of an item expressed by the probability that it will perform a required function under stated conditions for a stated period of time.

These definitions imply that the reliability describes the overall performance of the grid, and it can be seen that the reliability is strongly connected to the stability [45]. In the same sense as the stability is divided into steady-state and dynamic stability, the reliability is divided into two main areas: adequacy and security.

The adequacy is profoundly connected to the energy balance in the system and the steady-state stability [14]. This aspect of the reliability considers the systems ability to fulfil the load requirements and maintain the states of the system within operating limits [46]. This implies securing enough power production, both active and reactive, and the capability to transport the energy to the particular loads in the system. A considerable amount of research has been carried out regarding adequacy, and several indices have been developed [14]. These indices are used to evaluate the system and compare improvements in performance due to upgrades and changes made.

The adequacy is connected to the static operation of the grid, and system disturbances are not included in this part of the reliability analysis. The security is, on the other hand, strongly connected to the dynamic stability performance of the system, and the grid performance during disturbances is considered in this part of the reliability analysis [14].

Whereas adequacy is thoroughly investigated, the same amount of research has not been performed with security and further work must be done to develop security indices [14]. In this thesis, only the adequacy is investigated in the assessments performed. Henceforth, the word reliability will, therefore, only include the adequacy, not the security.

5.2 HLI, HLII and HLIII Studies

It is common to categorise reliability studies based on the parts of the power grid included in the study, often called hierarchy levels. There are three hierarchy levels; HLI, HLII and HLIII [14]. An overview of the three levels can be seen in fig. 5.1.

HLI is the first hierarchy level and includes the generation units in the power system. When an HLI- adequacy study is carried out, the generation units' ability to supply the load in a system is investigated. The system perspective of HLI studies can be seen in fig. 5.2a. Further, in HLII- studies, the transmission components are included, and the generation units ability to supply system load points is examined. The system perspective will then be as depicted in fig. 5.2b. Lastly, the third level, HLIII, includes all the components in the power system, and the generation units ability to supply customer load points is considered. For this level, the system perspective will be similar to the one for HLII, but

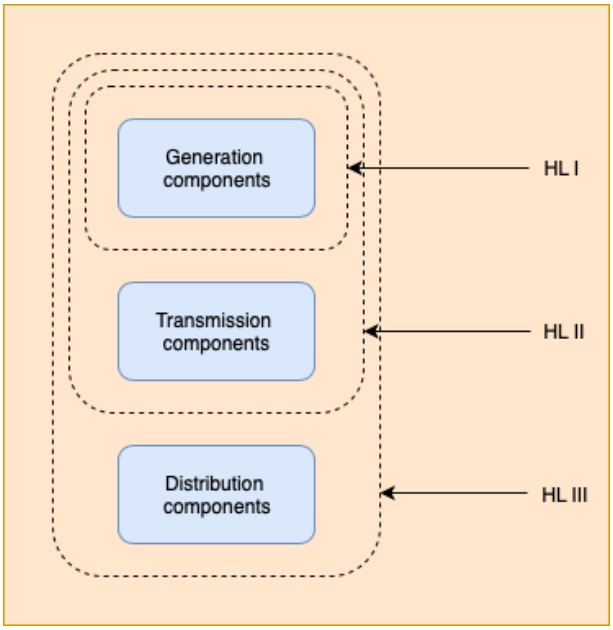

Figure 5.1: Hierarchy levels in adequacy analysis. Inspired by [14].

the distribution network from the bus to the individual customer will be included.

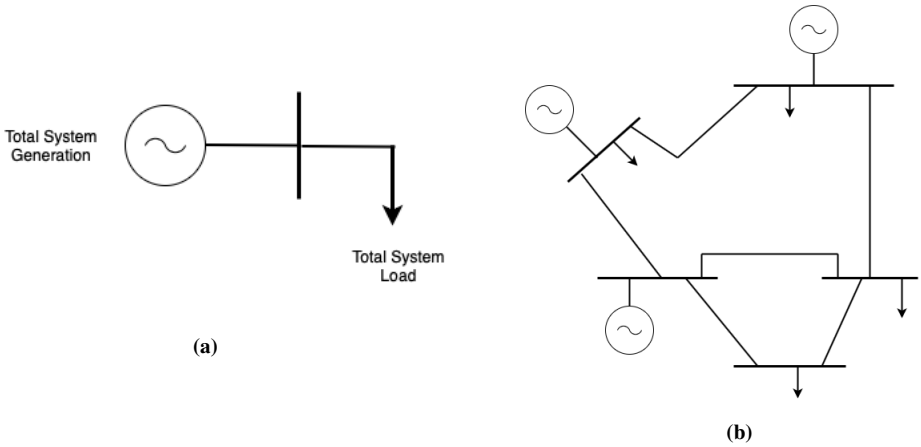

Figure 5.2: The system perspective in HLI (a) and HLII (b) studies. Inspired by [15].

5.3 Unavailability

The adequacy of a system can be evaluated based on the availability of the generating units, and their ability to supply the load can be examined. Conventional generators are modelled using a two-state generation model, where the unit is either fully available (Up) or not available/ out of service (Down). The unavailability of the generator can be calculated based on the expected failure and repair rate, denoted λ and μ, respectively. The failure and repair rate is the inverse of the Mean Time To Failure (MTTF) and Mean Time To Repair (MTTR). These values express the expected time between failures of the unit and expected time of repair in case of a fault. The formula expressing unavailability is given in eq. (5.1) [14].

$$Unavailability = FOR = \frac{\lambda}{\lambda + \mu} = \frac{MTTR}{MTTR + MTTF} = \frac{\sum[downtime]}{\sum[downtime] + \sum[uptime]} \tag{5.1}$$

The unavailability parameter is often called Forced Outage Rate (FOR) and describes the probability of a forced outage of the generator in the future, or the probability of Down-state. The FOR indicates the number of outages expected of a generator over some time. The probability of failure is, though, found to change over the lifetime of a unit. The bathtub curve, as can be seen in fig. 5.3, is a typical representation of this change [16]. As can be seen from the curve, the probability of failure is considerably larger during the burn-in and wear-out period, caused by a higher probability of infant mortality and wear-out failures. A component is not usually operated in a conventional system during the burn-in period, and most of the instances of infant mortality will only be experienced by the producer of the unit.

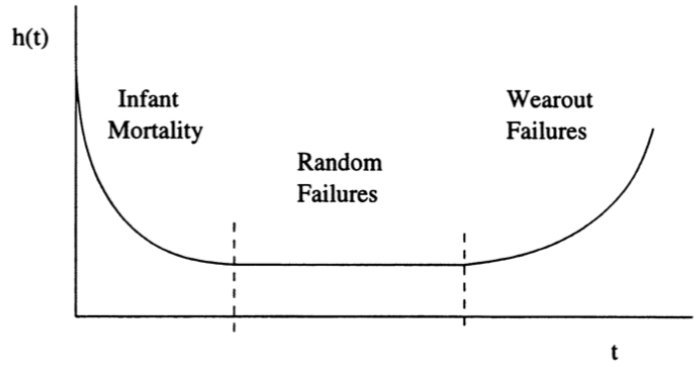

Figure 5.3: The bathtub-curve. Depicting the probability of outage in different periods of the lifetime of a component. [16]

During the useful life period of the generator, the probability of failure is assumed to be constant, only affected by random failures. The FOR will serve as a good indicator during this period. It must, however, be noted that the FOR value might be misleading for units entering the wear-out period, as the failure rate is likely to increase in this stage. In this thesis, the units in the microgrid at Rye is assumed to reside in the ”random failure”-state.

The power system is complex, and outage of one unit can affect other units causing dependent outages. Dependent outages are not rare, though hard to include in reliability analysis [14]. Such events will, therefore, not be included in the analysis in this thesis.

5.4 Derated states

Wind and solar sources do not have the same availability characteristic as conventional generators, where the unit is either fully available or out of service. The power produced by these sources varies due to variation in wind speed and solar irradiation. A multi-state model suits these characteristic better than a two-state model, as this allows for derated states where each state represents a given production level. A six-state model of a generator with derated states is depicted in fig. 5.4.

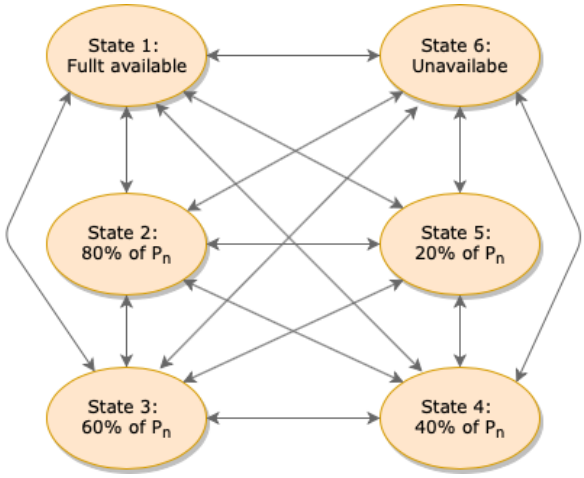

Figure 5.4: Six-state model of a generator with derated states.

When considering conventional generators, the probability of availability and unavailability is presented. For multi-state generation units, the probability of each of the derated states is given. The unavailable state includes both the probability of forced outage and the probability of no production due to weather conditions. An example of a generator with derated states is presented in table 5.1. This generator is a 100 kW machine with equal probability of each state and a forced outage rate of 10%.

Table 5.1: Probability table for a generator with derated states.

State	Available capacity [kW]	Probability [%]
1	100	15
2	80	15
3	60	15
4	40	15
5	20	15
6	0	25
		100

The different states in the multi-state model can be connected, and the likelihood of a transition from one state to another can be evaluated. The typical feature of these probabilities is dependent on the type of source. One can, for example, compare the characteristic of wind power and solar irradiation to find differences between a wind and solar generation unit. While the change in solar irradiation is continuous and the probability of the transition from, i.e. state 2 to 4, without entering state 3, is unlikely, a wind gust can cause such changes in a wind turbine generator [47].

Chapter 6

HLI- and HLII Probabilistic Adequacy Assessment

When utilising a probabilistic method, the generation and load units are treated as stochastic variables. This allows the including of the uncertainty of production level of renewable sources, demand level of loads and occurrence of faults and outages. Two different methods will be utilised when analysing the adequacy of the microgrid at Rye, one analytical method and one simulation method. The theory of these methods will be presented in the following chapter.

6.1 An analytical method for HLI adequacy assessment

In the analytical method, the reliability is analysed by means of probability distributions of the availability of the units in the system. This is done utilising the HLI hierarchy. The microgrid at Rye will, thereby, be modelled as a system only consisting of sources and loads, as presented in fig. 5.2a. The following section will present the theory needed to perform an HLI hierarchy adequacy assessment.

6.1.1 Capacity Outage Probability Table

A power system typically consists of several generation units, and to perform an adequacy analysis an overview of the generation availability of the whole system is needed. A Capacity Outage Probability Table (COPT) presents such an overview. This table includes the probability of different generating levels of all the generators in the system. By a recursive technique, the units are added sequentially, and a final model of the availability

of the whole system is obtained [14].

The formation of the COPT is most easily described by an example. Three two-state generators with a rated power of 5, 4 and 3 MW make up a small power system. The generator can either be Available (A) or Unavailable (U), resulting in eight possible states of the system. All of the units are said to have a FOR of 0.04, which gives A=0.96 and U=0.04 for each of the generators. The COPT for this system can be seen in table 6.1.

Table 6.1: Example COPT.

State i	Available capacity [MW]	Capacity Outage [MW] x_i	Individual prob. P(X=x_i)	Cumulative prob. P(X≥x_i)
1	12	0	AAA = 0.884736	1
2	9	3	AAU = 0.036864	0.115264
3	8	4	AUA = 0.036864	0.0784
4	7	5	UAA = 0.036864	0.041536
5	5	7	AUU = 0.001536	0.004672
6	4	8	UAU = 0.001536	0.003136
7	3	9	UUA = 0.001536	0.0016
8	0	12	UUU = 0.000064	0.000064

For every state of capacity outage, x_i, the individual probability, P(X=x_i), and cumulative probability, P(X≥x_i), were calculated. The individual probability displays the probability of capacity outage equal to the state x_i, while the cumulative probability shows the probability of the given or higher capacity outages. The cumulative probability can be calculated utilising eq. (6.1).

$$P(X \geq x) = \sum_{x_i \geq x} P(X = x_i) \tag{6.1}$$

As mentioned, the table is built using a recursive technique. The COPT will first only contain one generator. The other units are then included, one by one, by means of eq. (6.2) [14].

$$P(X \geq x_i) = (1 - FOR) \cdot P'(X \geq x_i) + FOR \cdot P'(X \geq x_i - C) \tag{6.2}$$

- P'(X≥ x_i) denotes the cumulative probability of capacity outage of X MW already present in the COPT.
- C denotes the capacity of the generator added to the table.

The expression in eq. (6.3) initialises the above equation.

$$P'(X \geq x_i) = \begin{cases} 1, & X \leq 0 \\ 0, & \text{otherwise} \end{cases} \tag{6.3}$$

If multi-state models of generators are added to the COPT, the term in eq. (6.2) must be slightly modified [14]. Eq. (6.4) displays the term used for this case.

$$P(X \geq x_i) = \sum_{j=i}^{n} p_i P(X \geq x_i - C_i) \tag{6.4}$$

- n is the number of derated states.
- C_i is the generator capacity in derated state i.
- p_i is the probability of the given generator capacity.

It must be noted that the states of the different generators are independent of each other in a COPT. An outage of one generator will, thus, not affect the outage of other units, despite that, a correlation between outage events can be found in a real-life system.

6.1.2 Probabilistic Indices

A set of developed probabilistic indices can be utilised when evaluating the adequacy of a system. It is common to divide these indices into two groups: risk indices and severity indices. The risk indices indicate the probability of loss of load, while the severity indices express the amount of load expected to be curtailed. The mathematical formulation of two risk indices, Loss Of Load Probability (LOLP) and Loss Of Load Expectation (LOLE), and one severity index, Expected Energy Not Supplied (EENS), will now be presented.

Loss Of Load Probability

LOLP presents the probability of the system being unable to supply a specified load with sufficient energy. The mathematical formulation can be seen in eq. (6.5) [15].

$$LOLP = P(X \geq C - L) \tag{6.5}$$

- X is the outage capacity.
- C is the installed capacity in the system.

- L is the load.

The LOLP is dependent on the load level in the system. Different loads yield different values of LOLP, and the mean and peak load are often applied as load levels in the calculations. A LOLP calculated using the peak load indicates the reliability during worst-case conditions, whereas the mean load might give a more realistic impression of the adequacy during normal conditions.

Loss Of Load Expectation

LOLE is the second risk index used in this study. This index presents hours within a year the system is expected to curtail the load [14]. A LOLE of 2.4 hrs/yr, equivalent to outage one day every tenth year, is often used as a standard adequacy criterion by power system planners [48].

The mathematical expression of this index can be found in eq. (6.6) [14].

$$LOLE = \sum_{i=1}^{8760} LOLP(i) = \sum_{i=1}^{8760} P(X \geq C - L(i)) \tag{6.6}$$

In the equation, the load might change each hour of the year, allowing the variation in load to be accounted for. However, a normal procedure is to calculate the LOLE using the yearly average load.

Expected Energy Not Supplied

EENS, also called Loss Of Energy Expectation (LOEE), is the only severity index used in this thesis. The index demonstrates the expected energy not delivered to the load [14]. The LOLP and LOLE do not account for the severity of outages. These indices treat a load curtail of 100 MW the same way as 10 kW, and severity indices, such as EENS, are often preferred, as these indices indicate the severity of the outage. The EENS can be calculated by means of eq. (6.7).

$$EENS = \sum_{i=1}^{N} E_i P_i = \sum_{i=1}^{N} \sum_{j=1}^{n(i)} L(j) - C(i) \tag{6.7}$$

- N is the number of capacity outage states.
- O_i is the capacity outage.

- E_i is the energy curtailed by capacity outage O_i.
- P_i is the probability of capacity outage O_i.
- n(i) is the number of load levels larger than the system capacity in state i.
- L(j) is the jth load level.
- C(i) is the system capacity during the ith capacity outage state.

The above expression is dependent on a load arranged in descending order. This load representation is called a load duration curve, and an example is depicted in fig. 6.1.

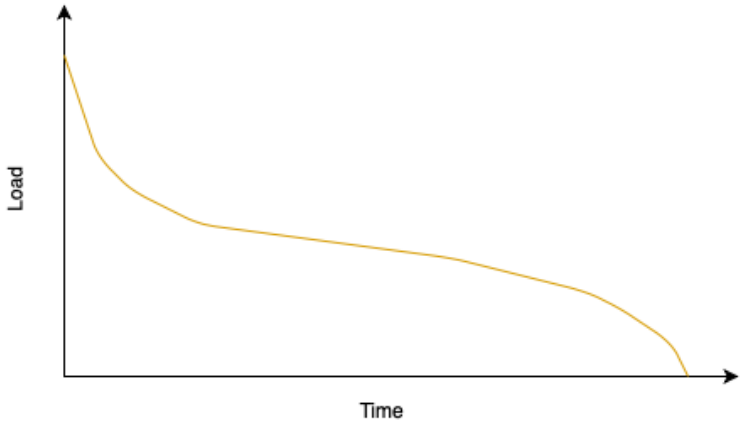

Figure 6.1: Example of a load duration curve.

6.1.3 Simplifications in the analytical method

A set of simplifications were carried out when conducting the described HLI adequacy assessment. A list of the most significant simplifications will follow:

- **Dependency of faults.** In power systems, faults are often connected, such that one fault causes other faults. This dependency was disregarded in this study.
- **Dependency of weather conditions.** Weather conditions are complex, and there can be detected a dependency between wind speed and solar irradiation. This dependency has not been accounted for in this study.
- **BESS as master.** The BESS acts as a master in the microgrid at Rye. Outages of the BESS will compromise a stable operation of the microgrid when no backup generator is included, despite that the remaining sources might have enough available capacity to supply the load. The crucial role of the BESS has not been included.

- **Derated faults.** Appearance of faults causing derated capacity of a unit is ignored in this study.
- **Reactive power.** In the microgrid at Rye, there will be a reactive power flow. This will be neglected when looking at the system adequacy.

6.2 Stochastic simulation methods for HLII adequacy assessment

Another way to capture the stochastic behaviour of the components is by stochastic simulations [49, 14]. When using this technique, the states of the units are determined based on random numbers. Similarly, the transition from one state to another is also dependent on random numbers. The coincidence of the numbers will result in different scenarios during simulations. A sufficient amount of simulations will thereby give a good indication of how the stochastic behaviour of the units affects the operation of the system. This type of stochastic simulation is often referred to as Monte Carlo Simulations (MCS).

The law of large numbers stands as one of the main pillars in MCS. This theorem describes that when performing an experiment numerous times, the average of the results will converge towards the expected value. The accuracy of the result exceeds with an increasing number of trials.

The technique of MCS is widely used in reliability assessments. Besides, the method easily allows the implementation of the HLII hierarchy level. Hence, the network connecting the units at Rye will be included in the MCS-analysis, resulting in a model more similar to fig. 5.2b. The following section will present theory about reliability analysis based on Monte Carlo Simulations.

6.2.1 Monte Carlo Simulations

As indicated, MCS are based on the generation of random numbers, which are used to compose different scenarios during the simulations. Random numbers can be generated through physical or mathematical methods [49]. The mathematical method is easily implemented on a computer. This method allows for reproducibility and is thereby not truly random and classifies as pseudorandom. The randomness must, therefore, be statistically tested by checking if the numbers are uniformly distributed (between [0,1]), if they are independent of each other and if the repeat period is sufficiently long.

Random numbers are often generated from a uniform distribution, with equal probability of generating any number. Several techniques, for example the Inverse Transform Method, are developed to generate random numbers from other distributions. These can be relevant for the MCS if, for instance, the failure of a unit is found to follow another distribution.

Monte Carlo Simulations can be performed in many different ways. The approaches are divided into two main categories: random and sequential [14]. In the random approach, the states of the units are decided solely on the random numbers generated, independent of the current state of the units. In the sequential approach, the states of the next state of the units are dependent on both the current state and the random number generated. This causes a chronological order of the steps in the simulation.

In literature, three MCS-methods are often presented: the state sampling method, the state duration method and the state transition method. In this thesis, the simulation framework is based on elements from the first two approaches, and a brief description of these techniques will follow.

State sampling method

In the state sampling method, a random number is generated for each unit in the system. The behaviour of the units are assumed to follow a uniform distribution between [0,1], and one random number is generated for each of the components in the system. The state of the unit is thereby determined based on the value of the corresponding number, using the following expression:

$$S_i = \begin{cases} A, & \text{if } U_i \geq FOR_i \\ U, & \text{if } 0 \leq U_i < FOR_i \end{cases}$$

In this expression S_i denotes the state of the ith unit, U_i the random number generated and A and U availability and unavailability, respectively. If the value of the random number is lower than the FOR of the unit, the state of the component will be set to U. Hence, the unit is unavailable. Similarly, a number above the FOR-value is equivalent to the availability of the unit during this time step. The system state is obtained by joining the states of all the units.

New numbers are generated for each time step in the simulation, deciding the state of the units at each step. The system state at each time step is solely dependent on the random number generated, and not affected by the state of the previous state. Hence, the scenarios simulated are non-sequential.

The state sampling method can also be utilised for systems consisting of multi-state components. A random number will be generated for these units as well. The value of the number will thereby determine the state of the unit. In the case of a unit with three states, fully available (A), derated state (D) and unavailable (U), the following expression is used:

$$S_i = \begin{cases} A, & \text{if } U_i \geq FOR_i + PDR_i \\ D, & \text{if } FOR_i \leq U_i < FOR_i + PDR_i \\ U, & \text{if } 0 \leq U_i < FOR_i \end{cases}$$

PDR$_i$ denotes the probability of the given derated state for the ith unit. Additional derated states can be added by using the probability of occurrence of these states.

State duration method

The state duration method is a sequential sampling method. A two-state component can be in two different states, either available or unavailable. Assuming independence of factors as weather conditions, the stochastic behaviour of the unit are single-handedly dependent on the occurrence of failures and repairs of failures. Hence, the duration of the states is dependent on the time to failure or the time to repair.

In the state duration method, the duration of each of the component states is simulated using the probability distribution of the expected failure rate, λ, and the expected repair rate, μ, for each of the component. These distributions are assumed to be exponential. Employing eq. (6.8a) and eq. (6.8b) a random value of time to failure (TTF) and time to repair (TTR) are generated.

$$TTF_i = -\frac{1}{\lambda_i} lnU_i \tag{6.8a}$$

$$TTR_i = -\frac{1}{\mu_i} lnU_i \tag{6.8b}$$

U$_i$ indicates a random number from a uniform distribution, while λ_i and μ_i are the expected failure and repair rate of the ith unit.

In the state duration method, an initial state of all the units in the system is decided. If a component is fully available, a random TTF will be generated, and this value determines the duration of the given state. In the same manner, a TTR will be generated whenever a unit is unavailable due to a fault. By continuous generation of TTFs and TTRs for the components in the system, the system state will be retrieved. A visualisation of how this is done is illustrated in fig. 6.2.

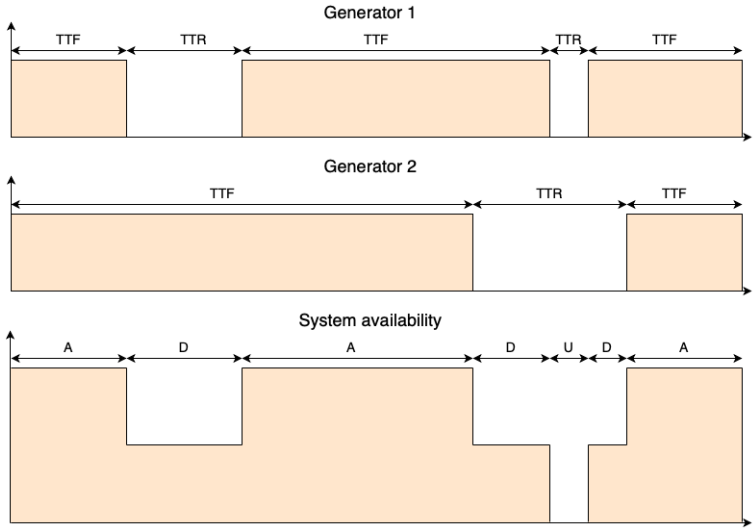

Figure 6.2: Illustration of the principle of the state duration method. TTF and TTR denoting the time to failure and time to repair, respectively. Further, A, D and U denotes the states of fully available, derated state and unavailable.

Furthermore, the method allows for multi-state units. For instance, if a three-state unit is in the derated state, the unit can whether change state to fully available or unavailable. The states of the three-state unit are depicted in fig. 6.3. λ_{23} represents the expected rate of transition from derated state to unavailable, while μ_{21} represents the expected rate of transition to fully available.

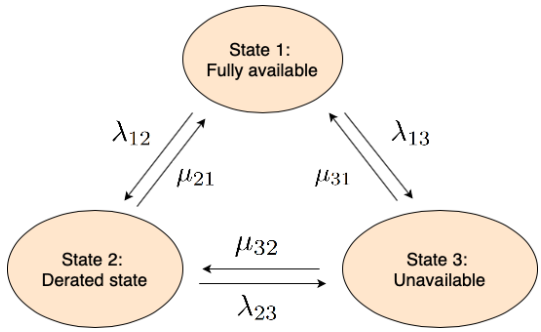

Figure 6.3: Transition between different states in a three-state model of a generator.

To determine the duration of the derated state and to which state the unit will transform, a random TTF_{23} and TTR_{21} are generated utilising λ_{23}, μ_{21} and two random numbers, U, from a uniform distribution. The transition time with the lowest value will occur first, and therefore determine the duration of the current state and the next state the unit will enter. A similar procedure can be utilised for units with several derated states.

6.2.2 Probabilistic Indices

The same adequacy indices as presented in section 6.1 will be utilised when performing an adequacy assessment based om MCS. The indices can, however, not be calculated in the same way. Consequently, new formulations of the indices will be presented in this section.

Loss Of Load Probability

[17] presents a method of LOLP calculation utilised for MCS. By MCS, the yearly production curve of the renewable sources can be generated. With a given load profile, the capacity of the energy storage units, and by then, the total capacity of the system, could be calculated. The result is depicted in fig. 6.4.

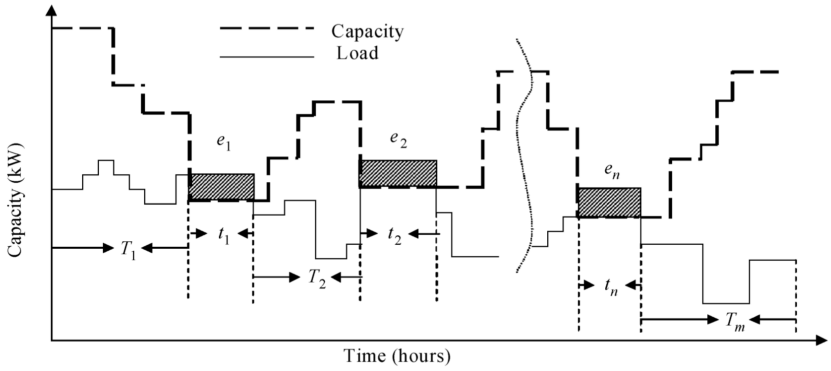

Figure 6.4: Capacity and load curve generated by Monte Carlo simulations in [17].

On the figure, the grey areas indicate the energy level of which the load is curtailed. During these periods the system is said to be in a risk state, and the time duration is denoted t_i. [17] then presents the calculation of LOLP, as shown in eq. (6.9).

$$LOLP = \frac{1}{8760N} \sum_{i=1}^{n(R)} t_i \tag{6.9}$$

- n(R) is the number of risk states.
- t_i is the time duration of which the system is in the ith risk state.
- N is a factor adjusting the LOLP in accordance with the time duration and time resolution of the simulated data.

Loss Of Load Expectancy

The calculation of LOLE is also presented in [17]. Assuming a time duration of the data set of one year and a time resolution of one hour, the LOLE can be calculated by employing eq. (6.10).

$$LOLE = \sum_{i=1}^{n(R)} t_i \tag{6.10}$$

Expected Energy Not Supplied

As previously described, the curtailed energy can be tracked during MCS as depicted in fig. 6.4. The EENS can be calculated by summing all the instances of curtailed load. These are coloured grey and marked with e_i in the figure. Further, the EENS can be calculated by using eq. (6.11).

$$EENS = \sum_{i=1}^{n(R)} e_i \tag{6.11}$$

6.2.3 Simplifications in the Monte Carlo Simulations

A set of simplifications were carried out when conducting the described HLII adequacy assessment. A list of the most significant simplifications will follow:

- **Dependency of faults.** In power systems, faults are often connected, such that one fault causes other faults. This dependency was disregarded in this study.
- **Derated faults.** Appearance of faults causing derated capacity of a unit is ignored in this study.
- **Reactive power.** In the microgrid at Rye, there will be a reactive power flow. Two adequacy assessments will be performed, one neglecting this power flow and one including the reactive power flow caused by the asynchronous generator in the wind turbine. Reactive power flow caused by other components in the microgrid will, however, be neglected in both assessments.

Chapter 7

Methodology

In chapter 4 four different control strategies were presented. The objective of this thesis is to compare the different strategies and how they impact the reliability of the microgrid at Rye. This will be done by performing two types of adequacy assessments, utilising both an analytical method and a stochastic simulation method, MCS.

An HLI-study will be performed using the analytical method. In this analysis, only the active power will be considered, as an implementation of reactive power flows is profoundly more complicated and time-consuming. The reactive power consumption of the wind turbine generator is thereby neglected in the analytical adequacy assessment.

As mentioned, an inclusion of the network layout of the microgrid is convenient when performing an adequacy assessment based on MCS. An HLII-study will, therefore, be performed when using the stochastic simulation method. Besides, the implementation of reactive power flows is considerably easier when using this method. This method allows for analysis where the reactive power consumption of the asynchronous generator is taken into account. Both an analysis only considering active power and an analysis considering both active and reactive power will be performed. This is to facilitate a more straightforward comparison between the results of the analytical and stochastic simulation method. Moreover, the effect of the reactive power consumption will be easy to detect when comparing the results of the two assessments.

The following chapter will constitute of a presentation of the availability parameters used in the assessments and a description of the datasets used in the analysis. Further, a review of the methodologies utilised in both the analytical and stochastic simulation method will be given. Finally, a description of how the efficiency of the fuel cell and the electrolyser were modelled in the simulations will be presented.

7.1 Forced Outage Rates

No FOR-value was assumed by the manufacturers for neither the two production units nor the two storage systems at Rye. Nor could literature present definite values of FOR for renewable energy sources and storage units. A proposal of realistic FOR-values for the four units is given in table 7.1. These values are determined based on example values of availability of different types of generators and units presented in [4], [5] and [6], as well as information about scheduled maintenance of the different components [50]. The availability parameters presented in literature were often given in MTTF and MTTR. The FOR-values were then calculated, employing eq. (5.1).

Table 7.1: Forced outage rates used for the units in the system. Based on values presented in [4], [5] and [6].

Unit	Forced Outage Rate	MMTF [hrs]	MTTR [hrs]
Wind turbine	0.018	2170	40
PV-system	0.015	3860	60
BESS	0.009	2190	20
HESS	0.028	1750	50
Transformers	0.004	3540	15
Backup generator	0.010	990	10

In addition, the table contains FOR, MTTF and MTTR values for the transformers and the backup generator. Once again, literature provides more information about typical values of availability for these units, and the FORs are decided based on the information given in [4], [5] and [6].

7.2 Production and consumption data

Production data from the renewable sources and consumption data from the farm at Rye constituted the bases of the analysis of the four cases. A year worth of measurements from the actual test site was provided by TrønderEnergi.

The operation of the PV-system was initiated in the spring of 2019. Hence, no production data was available before this time. Furthermore, improvements of the windmill operation and installation of new equipment on the farm have impacted the production and consumption levels. Consequently, it was decided to utilise data close in time, capturing the current production and consumption patterns. The dates covered in the datasets can be found in table 7.2

It must be noted that the datasets were organised according to the months of the year during the simulations. The simulations thereby followed the year, utilising data from the

Table 7.2: Dates of measured data from the microgrid at Rye.

Unit	Dates covered
Wind turbine	30^{th} of April 2019 - 29^{th} of April 202
PV-system	25^{th} of March 2019 - 25^{th} of March 2020
Load	29^{th} of April 2019 - 28^{th} of April 2020

first months of 2020 followed by measurements from months in 2019. Further explanation of how the simulations were performed will be described later in this chapter.

Due to maintenance and faults, measurements have not been recorded continuously. Instances of both losses of data and duplication of data were present in the datasets. Measures were taken to minimise the errors. A description of how the datasets were cleansed can be found in Appendix A.

7.2.1 Data from RenewablesNinja

To perform a thorough adequacy analysis a substantial amount of production data is needed. Additional wind and PV-data were, thus, simulated using the website www.renewables.ninja. This website provides a simulation tool which generates hourly output data from wind turbines and PV-systems. The following input parameters are needed when generating the wind data: location, year, capacity [kW], hub height and turbine model. When generating PV-data, the following parameters are needed: location, year, capacity, system loss, azimuth, tilt and if there are any type of tracking. The location was set to the coordinates of Rye farm, and output data from the years 2015-2019 was collected. The data was then compared with the measured production at Rye and found to correlate well, even though it was evident that the simulated yearly production was slightly higher than that measured at Rye.

The methodology used by RenewablesNinja when simulating production levels of the wind turbine and the PV-system is thoroughly described in [51] and [52].

7.3 Analytical method

The analytical method used in this thesis is based on the theory presented in section 6.1. The renewable sources in the microgrid are highly dependent on the weather conditions, causing the power output to fluctuate. Multi-state models were obtained to account for the fluctuating behaviour of the power sources in the adequacy assessment. Similarly, the capacity of the storage units fluctuates due to variations in energy deficit and excess in the system. To incorporate the two storage units in the analysis, they were, as well, modelled

as two multi-state sources. The establishment of these multi-state models is prerequisite to obtain the COPT, which is inevitable when calculating the reliability indices.

In this section, a description of the formulation of the multi-state models of the renewable sources and the storage units will be given.

7.3.1 Multi-state models

The establishment of the multi-state models is inspired by the work presented in [53]. The article presents a method of how to acquire a multi-state model of a wind turbine. A summary of the procedure is presented in fig. 7.1.

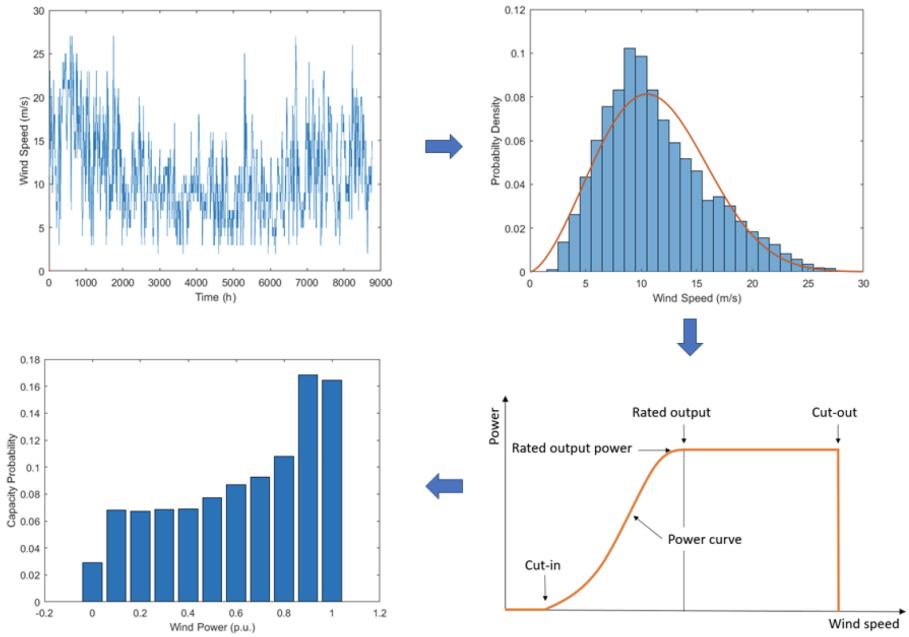

Figure 7.1: Procedure used when obtaining a multi-state model of a wind turbine. [18]

As can be seen from the figure, the method relies on a collection of wind speed data. This data is sorted, allowing for the formation of a probability density function of the different wind speeds. By combining this graph with the power curve of the wind turbine, the capacity probability of the wind power is obtained.

The described method assumes full availability of the unit, a FOR-value of 0% [53]. When generating the multi-state models of the units in Rye microgrid, the FOR-values presented in table 7.1 were added. This was done according to a method presented in [54]. The FOR-values were added to the probability of unavailability of the unit, and the remaining

probabilities were adjusted conforming the FOR-value added to the unavailability.

Renewable sources

The two renewable resources in the microgrid, a 225 kW wind turbine and an 82.8 kW PV-system, were modelled as two seven-state generating units. A similar approach as the one described above was utilised. Considering the production data of the two units were accessible, the data was categorised directly, attaining the capacity probability distribution of the two units forthright. Further, the designated FOR-values were added to the distributions.

Storage units

When performing the analytical adequacy assessment, both the storage units were modelled as sources. The BESS and HESS were modelled to have a full capacity of 216 kW and 100 kW, respectively. This reflects the rated power of the fuel cell and the maximum transferring power allowed by the converter in the BESS. The units were modelled such that whenever the energy capacity of the storages exceeded the rated power of the unit, the resource was set to fully available. The probability of derated states or unavailability was determined by the lack off capacity in the storage units. The BESS and HESS were modelled as four-state units, based on the experience from the specialisation project [19].

The microgrid at Rye is not running autonomously in June 2020, and the storage units are therefore not operated today. The multi-state models were thus based on simulated energy storage levels of the two units. Four models were developed in MATLAB, one for each of the cases presented in chapter 4. Using production data from the renewable resources and consumption data from the farm as input, the hourly energy level in the storage units were simulated, as depicted in fig. 7.2. By sorting and categorising the simulated data, four-state models of both the BESS and the HESS were established, one for each of the four control strategies.

7.3.2 Calculation of indices

To calculate the adequacy indices presented in chapter 5, the COPT was obtained. The LOLP, LOLE and EENS were then calculated by means of eq. (6.5), (6.6) and (6.7) using MATLAB-scripts. The scripts used to obtain the COPT and to calculate the indices are highly inspired by the work of [55]. When calculating the LOLP, the mean load was utilised as load-level, while the actual load profile acquired from the farm at Rye was used when calculating the LOLE and EENS. The algorithm used for these calculations of the LOLE and EENS can be seen in Appendix B.

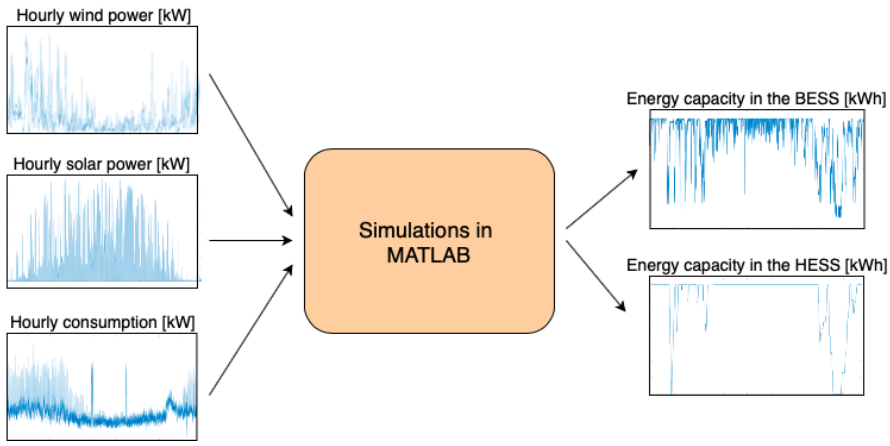

Figure 7.2: Illustration of how energy storage capacity of the BESS and the HESS was obtained.

7.3.3 HLI adequacy assessment

When performing the HLI adequacy assessment, the indices calculated for the different control strategies were compared. This was used to indicate how the choice of control strategy affected the reliability. Furthermore, both production data from the actual production site and data simulated by RenewablesNinja were utilised in the assessment. By performing the same adequacy assessment using different production data as input, one was able to observe the outcome for several years and validate the results of the assessment.

7.4 Stochastic simulation method

Monte Carlo Simulations was chosen as the stochastic simulation method. The methodology used when performing the MCS is based on the theory presented in section 6.2.

Four different models were developed in MATLAB to simulate the operation of the microgrid during different control strategies (the four control strategies presented in chapter 4). Hourly production and consumption data were used as input. The objective of the simulation was to calculate the energy capacity in the storage units and checked if the system were able to cover the load. Further, the adequacy indices were calculated. All this was carried out while accounting for the stochastic behaviour of failures of the components.

Elements from both the state sampling method and the state duration method were included in the simulations. Each hour of the simulation, eight random number was generated from a uniform distribution. If one of the numbers were found to be below the FOR-value of the designated unit, the given unit was set to unavailable. To make the MCS

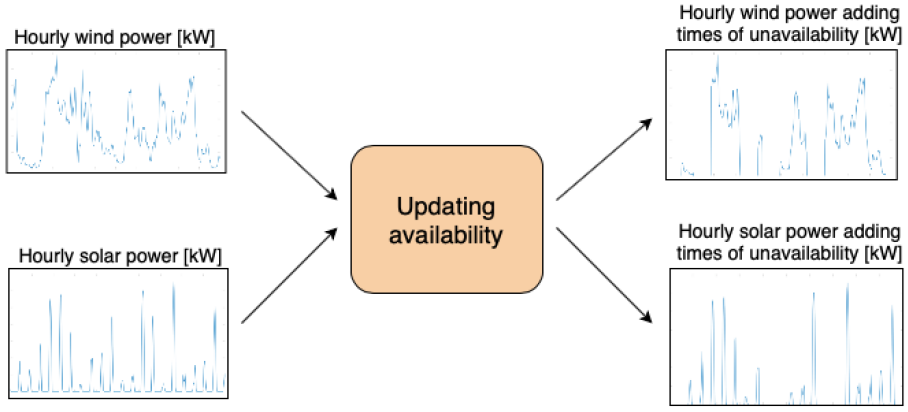

Figure 7.3: Example of how production data is updated when unavailability due to faults is accounted for.

sequential the units found to be unavailable were kept in this state for the same amount of hours as the MTTR. Thus, the state of the unit in the previous hour affects the state of the unit in the given hour. In fig. 7.3, the procedure is illustrated on two segments of production data from the wind turbine and the PV-system. As can be seen, the appearance of periods of unavailability is added in the graphs on the right-hand side.

Every hour of the year, the availability of the units were updated. Subsequently, the balance between consumption and production was calculated. In cases of excess energy, the surplus energy was divided between the two storage units in accordance with the given control strategy. However, in cases of limited capacity in the energy storage units, curtailment of some or all of the renewable production might be redeemed necessary.

During instances of deficit energy in the system, energy would be provided by the BESS, the HESS or both. The load sharing between the two units depended on the control strategy utilised. Further, if one or both of the storage units were unavailable, either due to faults or empty storage's, the backup generator was initiated. Additionally, if the system was unable to fulfil the load requirement load curtailment was necessary. These instances were registered and used as a foundation when calculating the LOLP, LOLE and EENS. The calculations were performed in accordance with eq. (6.9), (6.10) and (6.11). Fig. 7.4 depicts a simplified version of the algorithm used in the simulations.

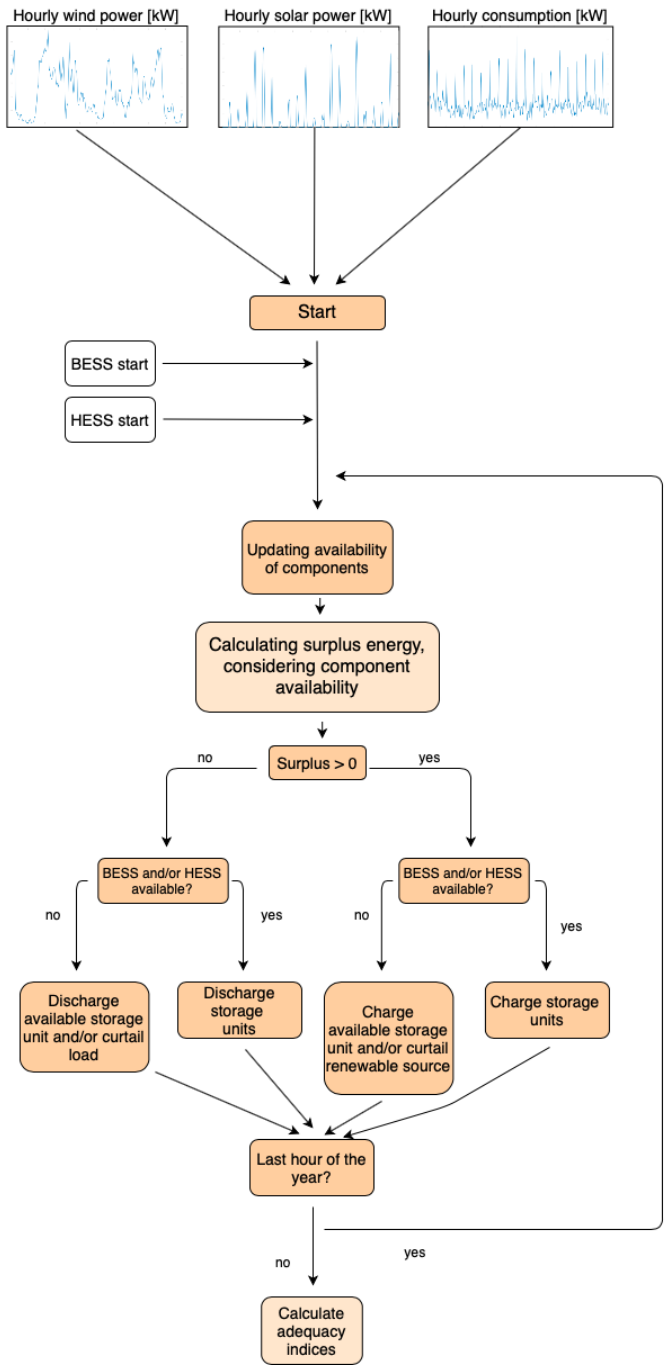

Figure 7.4: Simplification of the algorithm used in the simulations. The distribution of the energy is highly dependent on the control strategy used and will differ in the four cases.

7.4.1 HLII adequacy assessment only considering active power

An HLII adequacy assessment only considering active power flow in the microgrid was performed. The method described above was utilised. Firstly, the dataset containing the consumption data was used as input. Secondly, the production data from the two renewable resources were used as input. Six sets of data were utilised: the production data measured at Rye (presented in table 7.2) and five sets of production data simulated using RenewablesNinja (from 2015 to 2019).

For each of the MCS, the adequacy indices were calculated. Furthermore, 10 000 simulations were performed when carrying out the assessment. As a result, the distribution of the indices became available. However, the means of the calculated indices were used when analysing the adequacy of the system.

7.4.2 HLII adequacy assessment considering both active and reactive power

The same methodology, as described above, was used when performing the HLII adequacy assessment, where both active and reactive power was considered. The only adjustment was adding the reactive power flow in the models in MATLAB.

The asynchronous generator connected to the wind turbine has a significant reactive power consumption, causing reactive power flow in the system. This is the only reactive power flow accounted for in the analysis. Normally the lines and cables contribute to reactive power consumption and production, respectively. The short distances in the microgrid at Rye will, however, cause the amount of reactive power flow caused by the lines and cables to be negligible.

7.5 Modelling of HESS operating

An electrolyser, a gas container and a fuel cell constitutes the HESS in the simulations described previously in this chapter. During operation, the efficiency of the two units varies in accordance with the power level. In this section, the model of the varying efficiency utilised in simulations will be presented.

Electrolyser

The dynamic efficiency of the electrolyser is depicted in fig. 7.5. In the same figure, the linear approximation efficiency used in the simulations is depicted. A guesstimate of the efficiency during operating at power levels below 20% of nominal power is also included.

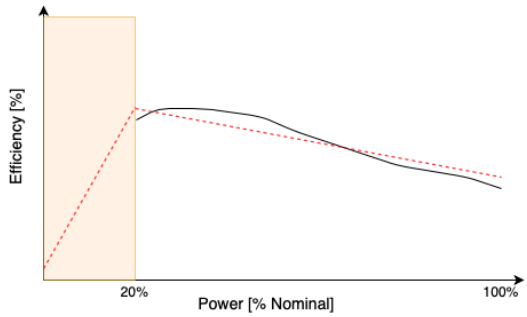

Figure 7.5: Linear approximation of the dynamic electrolyser efficiency. The dotted line represents the approximation.

The efficiency was thereby modelled as in eq. (7.1).

$$\eta_{EL,\%}(P_{EL}) = \begin{cases} 55.55 + 1.01 \cdot P_{EL}, & \text{if } P_{EL} < 11 \\ 55.15 - 0.14 \cdot P_{EL}, & \text{if } 11 \leq P_{EL} \leq 55 \end{cases} \tag{7.1}$$

Fuel cell

The linear approximation of the efficiency of the fuel cell can be seen in fig. 7.6.

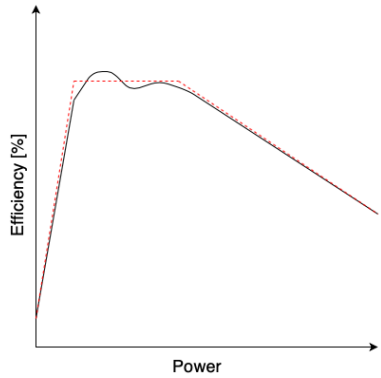

Figure 7.6: Linear approximation of dynamic fuel cell efficiency. The dotted line represents the approximation.

The mathematical formulation of the linear approximation can be seen in eq. (7.2).

$$\eta_{FC,\%}(P_{FC}) = \begin{cases} 34 + 1.19 \cdot P_{FC}, & \text{if } P_{FC} < 16 \\ 53, & \text{if } 16 \leq P_{FC} \leq 40 \\ 58.33 - 0.13 \cdot P_{FC}, & \text{if } 40 < P_{FC} \leq 100 \end{cases} \tag{7.2}$$

Chapter 8

Results

The adequacy assessment was performed using the two methods described in the previous chapter. First, reliability indices were calculated using the analytical method. By using measurements of production and consumption from the microgrid at Rye, as well as production data simulated using RenewablesNinja from 2015-2019, adequacy indices for all the four cases were calculated. Further, the same data was used to produce adequacy indices for each of the four control systems by means of MCS. Both simulations only accounting for active power and simulations accounting for both active and reactive power were conducted. This chapter will present three sets of adequacy indices. A discussion of how the results can be interpreted will follow in the next chapter.

8.1 HLI adequacy assessment using an analytical method

In this section the adequacy indices calculated by means of eq. (6.5), (6.6) and (6.7) will be presented. Nevertheless, the multi-state models of the units in the system will be presented first.

8.1.1 Multi-state models

The renewable sources were modelled to seven-state models, while the storage units were modelled as four-state models, as explained in section 7.3.1. Six sets of production data were used in the analysis; thus, six capacity probability tables were obtained for each of the sources. The COPTs of the can be seen in table 8.1 and 8.2.

The capacity outage probability tables contrived for the storage units were also dependent on the control strategy used in the system. The capacity available in the storage units

Table 8.1: COPTs of the PV-system using a seven-state model in case 1.

			Probability					
State	**Capacity In [kW]**	**Capacity Outage [kW]**	**Measured data from Rye**	**Data from RenewablesNinja from year:**				
				2019	**2018**	**2017**	**2016**	**2015**
1	82.8	0	0.0001	0.0031	0.0066	0.0049	0.0028	0.0017
2	74.52	8.28	0.0179	0.0340	0.0326	0.0271	0.0282	0.0231
3	57.96	24.84	0.0349	0.0413	0.0378	0.0454	0.0455	0.0412
4	41.4	41.4	0.0485	0.0561	0.0598	0.0589	0.0597	0.0539
5	24.84	57.96	0.0717	0.0837	0.0906	0.0859	0.0900	0.0884
6	8.28	74.52	0.3284	0.2590	0.2539	0.2541	0.2512	0.2682
7	0	82.8	0.4985	0.5229	0.5186	0.5236	0.5226	0.5237

Table 8.2: COPTs of the wind turbine using a seven-state model in case 1.

			Probability					
State	**Capacity In [kW]**	**Capacity Outage [kW]**	**Measured data form Rye**	**Data from RenewablesNinja from year:**				
				2019	**2018**	**2017**	**2016**	**2015**
1	225	0	0.0007	0.0000	0.0000	0.0000	0.0000	0.0000
2	202.5	22.5	0.0122	0.0000	0.0000	0.0000	0.0006	0.0000
3	157.5	67.5	0.0226	0.0100	0.0039	0.0015	0.0015	0.0076
4	112.5	112.5	0.0401	0.0232	0.0128	0.0167	0.0113	0.0418
5	67.5	157.5	0.0818	0.0676	0.0791	0.1017	0.0831	0.1106
6	22.5	202.5	0.3731	0.6870	0.6994	0.6866	0.6987	0.6577
7	0	225	0.4694	0.2123	0.2048	0.1935	0.2049	0.1822

at different times are determined by both the production data used and the control strategy. Hence, six COPTs were generated for each control strategy used. Table 8.3 and 8.4 presents the COPTs obtained for case 1, the original control system. Additional COPTs, for the other cases, ca be found in Appendix C.

Table 8.3: COPTs of the BESS using a four-state model in case 1.

			Probability					
State	**Capacity In [kW]**	**Capacity Outage [kW]**	**Measured data form Rye**	**Data from RenewablesNinja from year:**				
				2019	**2018**	**2017**	**2016**	**2015**
1	216	0	0.6961	0.8600	0.8748	0.8698	0.8589	0.8871
2	144	72	0.1251	0.0637	0.0600	0.0766	0.0826	0.0706
3	72	144	0.1717	0.0660	0.0554	0.0439	0.0485	0.0328
4	0	216	0.0107	0.0104	0.0098	0.0097	0.0100	0.0095

Table 8.4: COPTs of the HESS using a four-state model in case 1.

			Probability					
State	**Capacity In [kW]**	**Capacity Outage [kW]**	**Measured data form Rye**	**Data from RenewablesNinja from year:**				
				2019	**2018**	**2017**	**2016**	**2015**
1	100	0	0.7663	0.8955	0.9172	0.9264	0.9193	0.9319
2	66.66	33.33	0.0158	0.0087	0.0012	0.0016	0.0051	0.0007
3	33.33	66.66	0.1899	0.0008	0.0007	0.0017	0.0048	0.0393
4	0	100	0.0281	0.0950	0.0809	0.0704	0.0708	0.0281

8.1.2 System COPT

As explained in section 6.1, a COPT including all the sources in the system has to be obtained to calculate the adequacy indices using the analytical method. Six datasets of production and four control strategies resulted in 24 different COPTs. As the COPTs included two seven-state models of the renewable sources, two four-state models of the storage units and a two-state model of the backup generator, each of the COPTs contained 1568 states. Hence, the system COPTs used in the calculations of the indices will not be presented in this thesis, but can be obtained by combining the COPTs of the different units.

8.1.3 Adequacy indices

LOLP

The loss of load probability was calculated by means of eq. (6.5). Different datasets of production data, and thereby different COPTs were used in the calculations. The results are presented in table 8.5. In the table, the LOLPs are categorised based on the input data used and the control strategy utilised during simulations of the storage capacities.

Table 8.5: LOLP-values calculated by means of the analytical method.

Case	**Measured data from Rye**	**Data from RenewablesNinja from year:**				
		2019	**2018**	**2017**	**2016**	**2015**
1	1.167e-06	1.6401e-06	1.2543e-06	1.0276e-06	1.1225e-06	3.8517e-07
2	1.058e-06	1.4824e-06	1.1888e-06	3.9326e-07	3.1799e-07	3.0196e-07
3	1.167e-06	1.6401e-06	1.2543e-06	1.0276e-06	1.1225e-06	3.8517e-07
4	1.1999e-04	9.2924e-06	6.8239e-06	3.9302e-06	6.0322e-06	3.6494e-07

In fig. 8.1, the values are depicted in a bar chart. It is evident from the graph that the

control strategy used in case 4, the peer-to-peer strategy, results in considerably higher LOLP-values when utilising the production data measured at Rye. The LOLP differs from 0.0001058 % for case 2, to 0.011999 % for case 4. It can, however, be observed that the difference between the indices is considerably lower when the simulated production data from RenewablesNinja is used. In 2016, 2017, 2018 and 2019 the LOLP is still higher for case 4. Nevertheless, in 2015 the LOLP for case 4 is lower than the case 1 and 3-value.

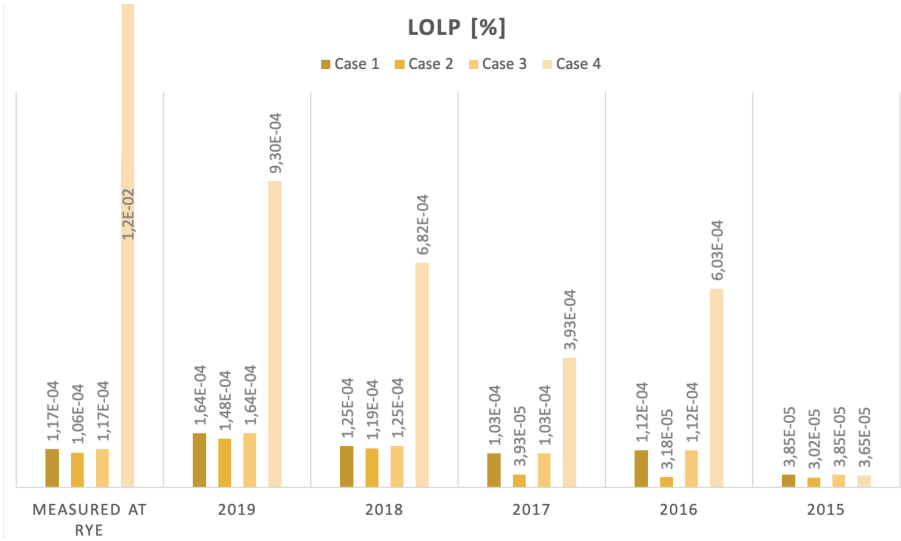

Figure 8.1: Bar chart presenting the LOLP-values calculated by means of the analytical method. Values are stated in %.

Additionally, it can be observed that case 1 and 3 has the same value LOLP in all calculations. This is because the simulations of the two cases resulted in the same COPTs for both storage units, and the same LOLPs. Further in this section, it will become evident that all indices are equal for case 1 and 3 when utilising the analytical method.

Furthermore, it is evident that the control strategy in case 2 results in lower LOLP when using the analytical method. Regardless of input data, the bars representing case 2 are lower than for all other cases.

LOLE

The loss of load expectancy was calculated using eq. (6.6). The calculated LOLE indices can be found in table 8.6.

Anew, the indices are visualised in a bar chart, shown in fig. 8.2. As can be seen, the peer-to-peer strategy causes the highest LOLE, ranging from 0.0396 to 1.1172 hrs/yr. It must, however, be noted that these values are all below the standard reliability criterion of 2.4

Table 8.6: LOLE-values calculated by means of the analytical method. Stated in hrs/yr.

Case	Measured data from Rye	Data from RenewablesNinja from year:				
		2019	2018	2017	2016	2015
1	0.0128	0.0174	0.0134	0.0111	0.0120	0.0043
2	0.0115	0.0157	0.0127	0.0044	0.0036	0.0034
3	0.0128	0.0174	0.0134	0.0111	0.0120	0.0043
4	1.1172	0.0991	0.0732	0.0429	0.0649	0.0396

hrs/yr. Based on these indices, one can, therefore, argue that sufficiently good reliability can be attained in all cases.

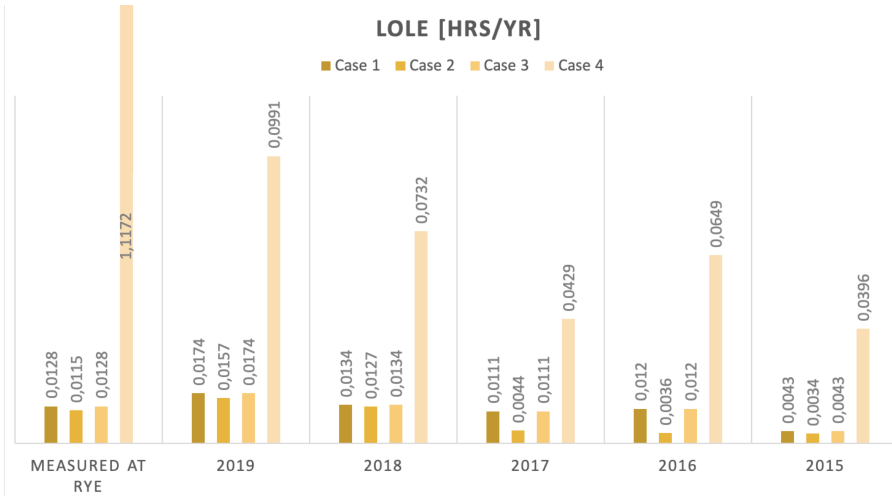

Figure 8.2: Bar chart presenting the LOLE-values calculated by means of the analytical method. Values are stated in hrs/yr.

The same pattern as found in the LOLP-values can be detected in the LOLE: case 4 causes the highest values, case 2 results in the lowest LOLE and case 1 and 3 have the same values.

EENS

Eq. 6.7 was used to calculate the expected energy not served. The results are listed in table 8.7.

The same results are presented in fig. 8.3. From the chart, it is evident that the control strategy in case 4 causes the highest EENS. Once more, the value calculated for case 4

Table 8.7: EENS-values calculated by means of the analytical method. Stated in kWh/yr.

Case	Measured data from Rye	Data from RenewablesNinja from year:				
		2019	**2018**	**2017**	**2016**	**2015**
1	0.1452	0.2016	0.1556	0.1283	0.1394	0.0496
2	0.1311	0.1822	0.1475	0.0505	0.0410	0.0390
3	0.1452	0.2016	0.1556	0.1283	0.1394	0.0496
4	13.0694	1.1487	0.8487	0.4925	0.7515	0.4509

using the measured production from Rye is considerably higher than the EENS calculated using data from RenewablesNinja. Using the peer-to-peer strategy, the EENS ranges from 0.4509 to 13.0694 kWh/yr.

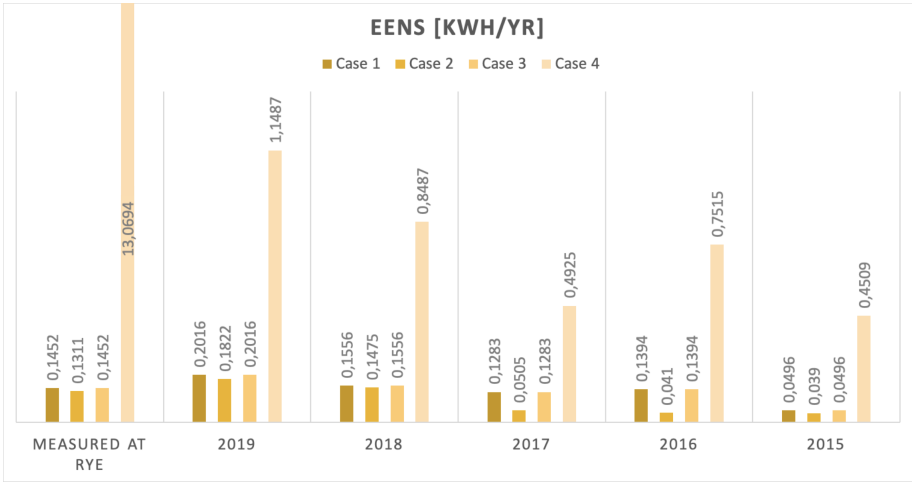

Figure 8.3: Bar chart presenting the EENS-values calculated by means of the analytical method. Values are stated in kWh/yr.

Furthermore, the EENS-values show, similar to the LOLP and LOLE, that the demand-side management implemented in the control strategy in case 3 causes lower values of the adequacy indices when using the analytical method. Based on these results, one can thereby argue that this control strategy cases better reliability in the microgrid.

8.2 HLII adequacy assessment using MCS, neglecting reactive power flow

In this section, the results of the first MCS neglecting reactive power will be presented. The simulations were performed as described in section 7.4 and the indices were calculated using eq. (6.9), (6.10) and (6.11). Additionally, a count of the start and stop-cycles needed for the electrolyser and the fuel cell during the simulations were collected. The values can be used as an indication of how the control strategies in the four cases affect the degradation and lifetime of the components in the hydrogen system.

8.2.1 Adequacy indices

8.2.2 Distribution of indices

As described in section 7.4 10 000 simulations were performed for each of the sets of production data. Hence, each of the indices was obtained 10 000 times. In fig. 8.4, 8.5, 8.6 and 8.7 depicts the distributions of the LOLPs. These plots represent the distribution acquired when the measured data from Rye was used as input in the simulations and will pose as examples of how the distributions of the indices look.

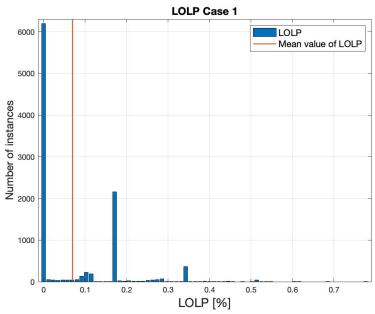

Figure 8.4: Distribution of recorded LOLP-values during simulations of case 1 using data measured at Rye.

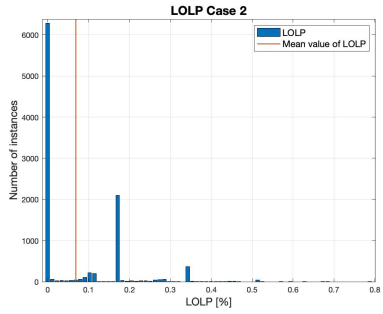

Figure 8.5: Distribution of recorded LOLP-values during simulations of case 2 using data measured at Rye.

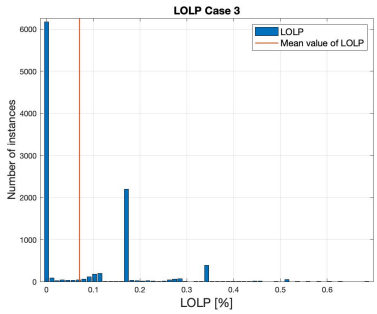

Figure 8.6: Distribution of recorded LOLP-values during simulations of case 3 using data measured at Rye.

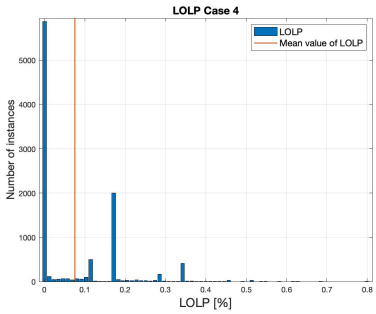

Figure 8.7: Distribution of recorded LOLP-values during simulations of case 4 using data measured at Rye.

The appearance of a LOLP value of 0% is most common. Moreover, there is a spike at a LOLP of 0.18% in all of the four cases. Furthermore, the mean value of the distribution is marked with a red line. Similar characteristics were found in the other index distributions, and they will not be displayed in this thesis.

LOLP

The mean values of the LOLP distributions of the 24 MCS performed are presented in table 8.8.

Table 8.8: LOLP-values calculated using MCS (neglecting reactive power flow in the microgrid).

Case	Measured data from Rye	Data from RenewablesNinja from year:				
		2019	2018	2017	2016	2015
1	0.0007	0.00063	0.00063	0.00063	0.00062	0.00063
2	0.0007	0.00063	0.00063	0.00062	0.00063	0.00062
3	0.0007	0.00061	0.00062	0.00061	0.00061	0.00061
4	0.0008	0.00064	0.00064	0.00064	0.00061	0.00062

Fig. 8.8 depicts the same results in a bar chart. It must be noted that the chart presents the LOLP-values in %, whilst the results are given in decimals in table 8.8.

Similar to the results produces by the analytical method, these results indicate that the production data collected from Rye results in somewhat higher indices than when simulated data from RenewablesNinja is utilised. This can be explained by the slightly higher annual production level detected in the simulated production data.

Whereas the LOLP-values produced by the analytical method gave quite unambiguous

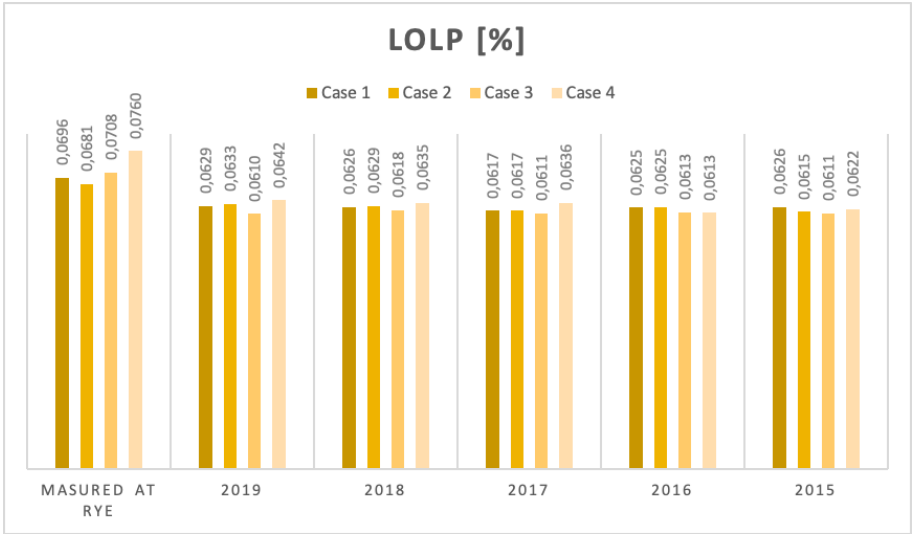

Figure 8.8: Bar chart presenting the LOLP-values calculated using MCS (neglecting reactive power flow in the microgrid).

indications of performance of the four control systems, these results are more unclear. The peer-to-peer strategy, case 4, seems to perform poorer than the other cases during simulations with measured data and data from 2019, 2018 and 2017. However, it can be observed that case 4 scores better in 2016 and 2015.

Additionally, it can be observed that case 3 performs better than the three other cases in all MCS performed with data from RenewablesNinja as input. Nevertheless, both case 1 and case 2 presents a lower mean LOLP during simulations using production data measured at Rye. The variations are, though, small, varying from 0.0681% for case 2 to 0.0708% for case 3.

Another interesting finding is the weak performance of the system using a control strategy with demand-side management, case 2. Whereas case 2 systematically performed better than case 1 during the analytical calculations, the LOLP is slightly higher than that of case 1 in 2019 and 2018 and similar to case 1 in 2017 and 2016. Case 2 do, however, perform better than case 1 in 2015 and when utilising data measured at Rye. These results show the importance of the chronology of the events, which is included in the MCS, but not accounted for when using the analytical method. Load-shifting can be complicated, and though the intention is to move peak loads to periods with lower power demand, this can be difficult. Thus, big loads can be shifted to periods of even higher load demand. In autonomous microgrids a load shift can also result in higher demand during times of even lower energy capacity in the storage units, affecting the reliability negatively. This may have occurred in this instance.

LOLE

The LOLP in the MCS is calculated by dividing the LOLE by 8760 (the number of hours in a year). Hence, the same patterns will be found in the LOLP- and LOLE-results. The obtained LOLE-values are presented in table 8.9.

Table 8.9: LOLE-values calculated using MCS (neglecting reactive power flow in the microgrid). Values stated in hrs/yr.

Case	Measured data from Rye	Data from RenewablesNinja from year:				
		2019	2018	2017	2016	2015
1	6.0970	5.5101	5.4825	5.4037	5.4735	5.4856
2	5.9691	5.5483	5.5065	5.4064	5.4776	5.3877
3	6.2020	5.3442	5.4135	5.3518	5.3694	5.3551
4	6.6548	5.6226	5.5643	5.5704	5.3661	5.4460

The results are depicted in fig. 8.9. It is evident that regardless of control strategy, the LOLE will exceed the desired level of 2.4 hrs/yr. The value varies from 5.3518 to 6.6548, approximately 2.5 times higher than the standard criteria of power system planners. Nevertheless, the REMOTE-project indicated a goal of availability above 98%. This is equivalent to a LOLE below 173.4 hrs/yr. The results show that this goal is well accomplished.

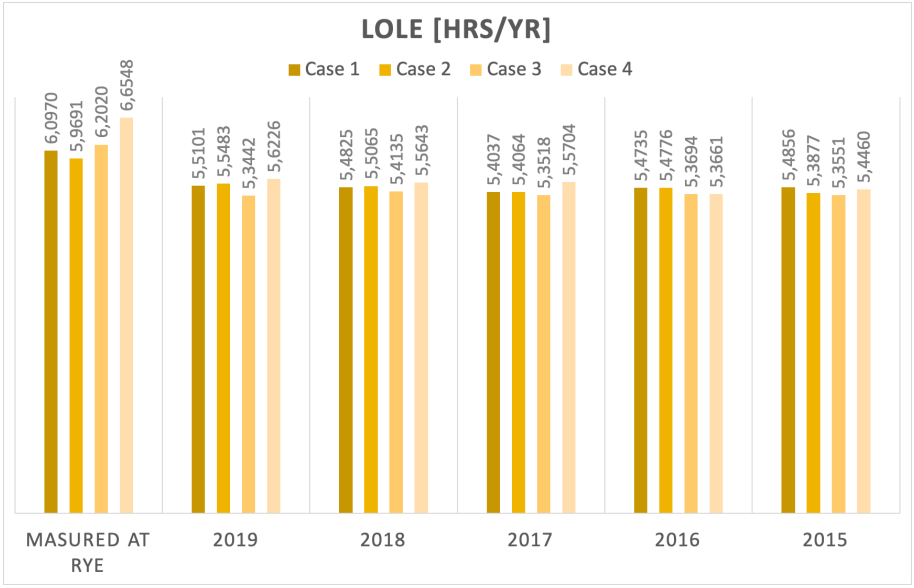

Figure 8.9: Bar chart presenting the LOLE-values calculated using MCS (neglecting reactive power flow in the microgrid).

EENS

Whereas the LOLP and the LOLE are mathematically bound by a factor of 8760, the EENS is calculated independently of these indices. The severity index will, therefore, present other variations than those presented above. The EENS-indices are presented in table 8.10.

Table 8.10: EENS-values calculated using MCS (neglecting reactive power flow in the microgrid). Values stated in kWh/yr.

Case	Measured data from Rye	Data from RenewablesNinja from year:				
		2019	2018	2017	2016	2015
1	135.74	111.11	150.77	387.85	231.45	123.35
2	158.44	325.44	133.68	121.48	130.63	113.93
3	147.46	111.18	123.59	311.23	154.80	112.56
4	135.34	110.35	109.28	110.01	103.97	108.51

The same results are depicted in fig. 8.10. Once again, the results from the MCS do not present a clear indication of which of the four control strategies that provide in the best adequacy performance.

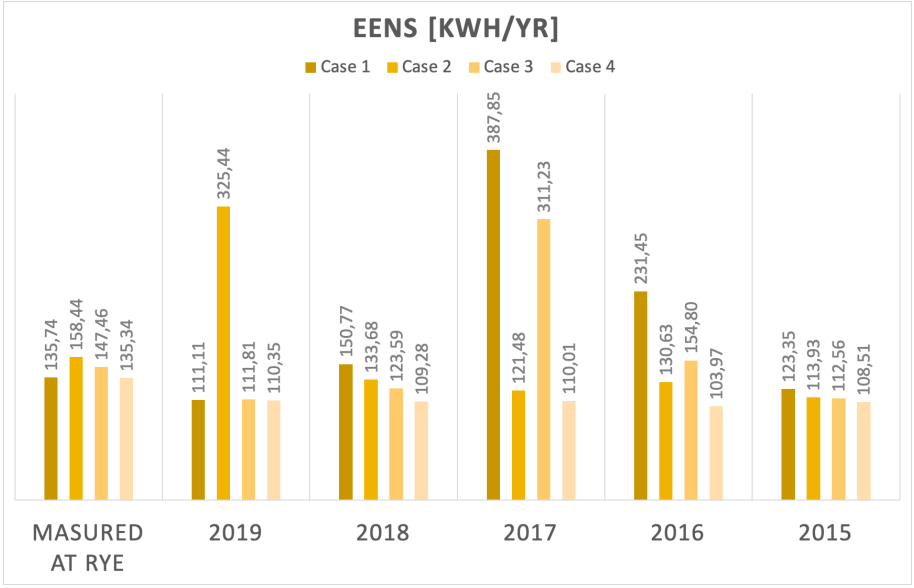

Figure 8.10: Bar chart presenting the EENS-values calculated using MCS (neglecting reactive power flow in the microgrid).

From the graph in fig. 8.10, it is evident that in 2018, 2017, 2016 and 2015, the demand-side management implemented in case 2 result in lower load curtail than in case 1. It can

be assumed that despite the increase in hours of load curtail expected, observed in the LOLE indices, the curtails appear at more convenient times, resulting in lower severity. However, the EENSs of case 2 are considerably higher than case 1 in 2019 and slightly higher when the measured data is used as input.

When looking at the severity indices, it is evident that the peer-to-peer control strategy in case 3 provides lower load curtail than the other cases.

Start and stop-cycles in the hydrogen system

During the simulations, the number of starts of the electrolyser and the fuel cell were recorded. The mean value of the 10 000 simulations are presented in table 8.11 and 8.12 and give a good indication of the degradation the hydrogen units are exposed to.

Table 8.11: Mean of number of starts of the electrolyser needed in the MCS (neglecting reactive power flow in the microgrid).

Case	Measured data from Rye	Data from RenewablesNinja from year:				
		2019	**2018**	**2017**	**2016**	**2015**
1	1056.4	1422.3	1486.6	1420.7	1163.6	1675.2
2	1083.7	1440.6	1509.3	1473.3	1201.4	1685.2
3	1030.1	1425.0	1469.8	1443.8	1184.0	1654.7
4	3718.5	5054.3	5265.8	5192.9	4962.6	5511.7

Table 8.12: Mean of number of starts of the fuel cell needed in the MCS (neglecting reactive power flow in the microgrid).

Case	Measured data from Rye	Data from RenewablesNinja from year:				
		2019	**2018**	**2017**	**2016**	**2015**
1	202.5	83.3	88.6	72.9	78.1	53.5
2	100.4	36.8	35.6	28.5	32.3	24.5
3	113.2	42.1	54.9	35.1	47.7	31.2
4	4909.9	3573.9	3361.6	3435.6	3666.0	3117.8

From the two tables, it is evident that the control strategy in case 4 causes a considerable increase in starts of both the electrolyser and the fuel cell. Compared with case 1, the amount of starts of the electrolyser is two or three times as high in case 4, and about 30 times as high for the fuel cell. Consequently, the degradation of the hydrogen system is substantially greater in case 4.

Further, it can be observed that the demand-side management in case 2 causes the average number of starts of the electrolyser to decrease compared to both case 1 and 3. The opposite pattern can, however, be observed for the fuel cell. Here the numbers of start needed

are lower in case 2 than in case 1 and 3. Thus, the degradation of the electrolyser is higher during case 2 but lower for the fuel cell.

No clear distinction is detectable in the number of starts of the electrolyser in case 1 and 3. Which of the two cases resulting in the lowest number of starts differs in the six scenarios. A clear pattern can, nevertheless, be observed for the fuel cell. Fewer starts are needed during case 3.

8.3 HLII adequacy assessment using MCS including reactive power

To detect the impact of the reactive power consumption of the wind turbine generator, MCS were performed with simulations that accounted for this reactive power flow. The results from these MCS will be presented in this section.

8.3.1 Adequacy indices

LOLP and LOLE

The mean LOLP- and LOLE-values are presented in table 8.13 and 8.14.

Table 8.13: LOLP-values calculated using MCS (including reactive consumption of the wind turbine generator).

Case	Measured data from Rye	Data from RenewablesNinja from year:				
		2019	2018	2017	2016	2015
1	0.0007	0.00064	0.00062	0.00061	0.00060	0.00059
2	0.0007	0.00064	0.00062	0.00062	0.00062	0.00061
3	0.0007	0.00064	0.00062	0.00061	0.00062	0.00060
4	0.0008	0.00066	0.00064	0.00063	0.00064	0.00063

From the tables, it is evident that the reactive power flow caused by the asynchronous generator has only a minor impact on the adequacy of the microgrid. In all the cases the LOLP varies from 0.0593 to 0.0774% and the LOLE from 5.1940 to 6.776 hrs/yr. These values are in the same range as the risk indices calculated when neglecting the reactive power.

Fig. 8.11 and 8.12 depicts bar charts of the LOLPs and LOLEs, respectively.

In similarity to that discovered in section 8.2, the simulations using data from RenewablesNinja as input result in lower values of LOLP and LOLE. In addition, the same pat-

Table 8.14: LOLE-values calculated using MCS (including reactive consumption of the wind turbine generator). The values are stated in hrs/yr.

Case	Measured data from Rye	Data from RenewablesNinja from year:				
		2019	**2018**	**2017**	**2016**	**2015**
1	6.2782	5.6253	5.4477	5.3736	5.2929	5.1940
2	6.3821	5.5689	5.4413	5.4623	5.4466	5.3525
3	6.1416	5.5880	5.3987	5.3263	5.3890	5.2555
4	6.7776	5.7666	5.5846	5.5459	5.5696	5.4767

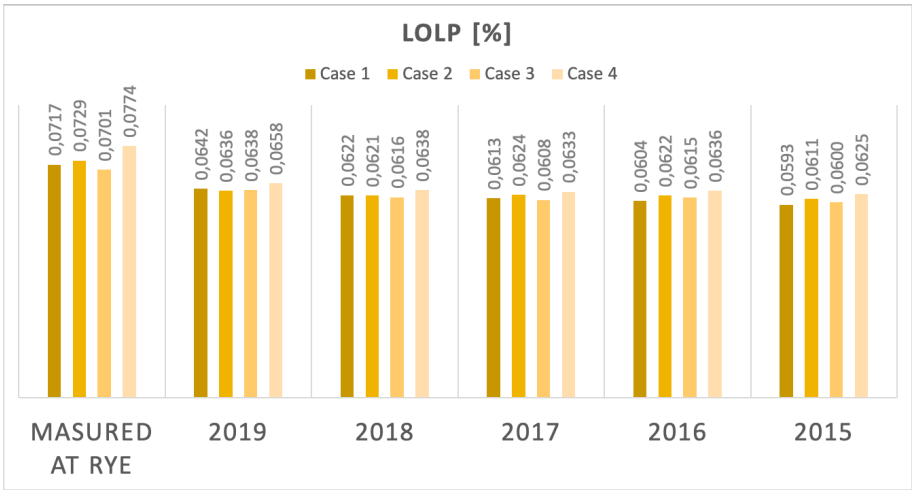

Figure 8.11: Bar chart presenting the LOLP-values calculated using MCS (including reactive power consumption of the wind turbine generator).

terns can be found in the bar charts. Firstly, it can be observed that the LOLP- and LOLE-values of case 4 are somewhat higher than the other indices. Secondly, the demand-side management implemented in case 2 causes slightly higher indices in some of the scenarios presented. Using input data from 2017, 2016, 2015 and data measured at Rye, case 2 has higher LOLP and LOLE than case 1, whereas the values are approximately similar in 2019 and 2018. Finally, a varying performance of the control strategy in case 3 can be observed. Using measured data from Rye, data from 2018 and 2017, the simulations of case 3 produce the lowest indices. However, in both 2019 and 2015, either case 1 or case 2 performs better than case 3.

Once again, it must be noted that all the risk indices produced will fulfil the desired availability of 98% with a good margin.

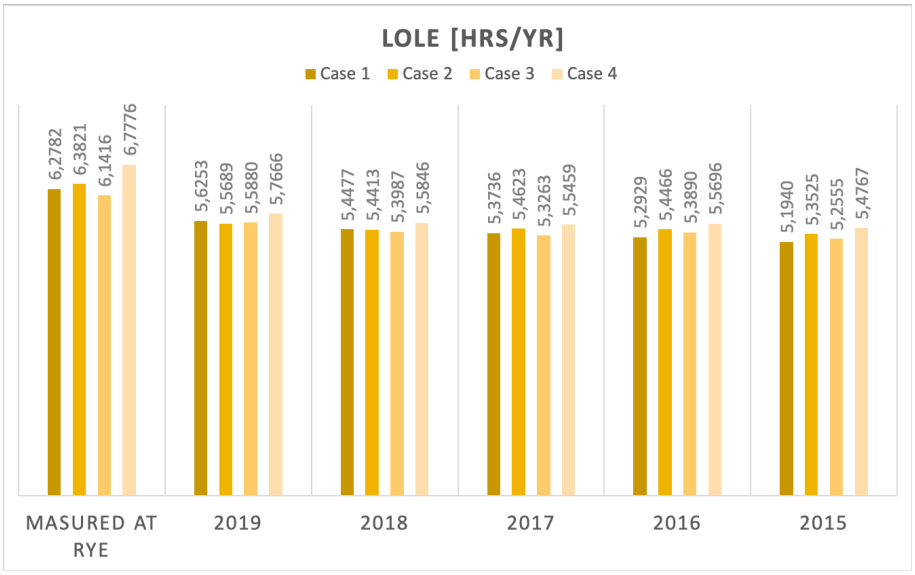

Figure 8.12: Bar chart presenting the LOLE-values calculated using MCS (including reactive power consumption of the wind turbine generator).

EENS

The EENS-value calculated for the four cases are presented in table 8.15, and the same results are depicted in fig. 8.13.

Table 8.15: EENS-values calculated using MCS (including reactive consumption of the wind turbine generator). The values are stated in kWh/yr.

Case	Measured data from Rye	Data from RenewablesNinja from year:				
		2019	2018	2017	2016	2015
1	141.66	113.42	139.22	130.67	220.94	118.54
2	135.16	120.29	108.26	108.97	108.04	108.22
3	159.38	118.12	133.01	152.70	134.63	111.64
4	137.60	112.68	109.48	100.28	109.13	108.76

Anew, no clear equivalence can be drawn from the values of the risk and severity indices. However, the results presented in fig. 8.10 are more similar to that presented by these EENS-values. One can thereby argue that the reactive power flow has limited impact on the severity of the load curtail.

Low EENS-values during simulations using the control strategy in case 4 suggest that the load curtails occur at more favourable hours. Further, the severity of the load curtails in case 2 are less than that found for both case 1 and 3 in all scenarios, except in 2019.

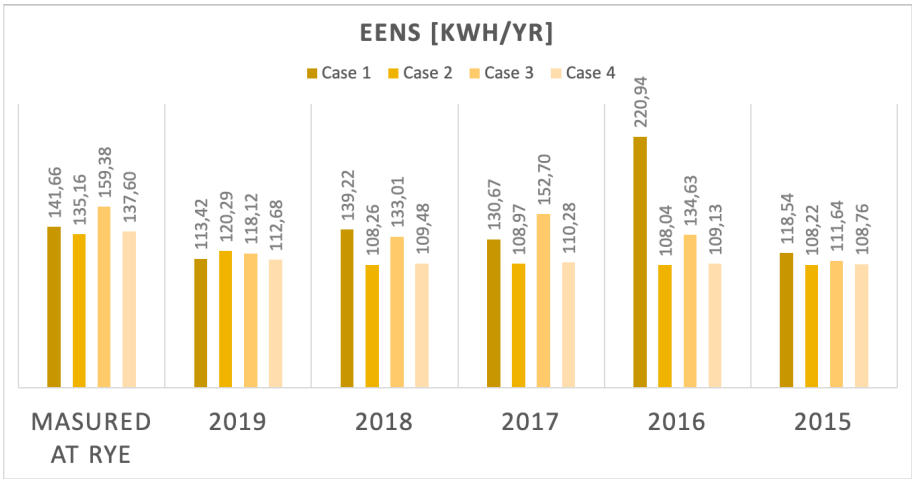

Figure 8.13: Bar chart presenting the EENS-values calculated using MCS (including reactive power consumption of the wind turbine generator).

Start and stop-cycles in the hydrogen system

The numbers of starts needed by the electrolyser and fuel cell are also similar to that presented in section 8.2. The numbers are shown in table 8.16 and 8.17.

Table 8.16: Mean of number of starts of the electrolyser needed in the MCS (including reactive power consumption of the wind turbine generator).

Case	Measured data from Rye	Data from RenewablesNinja from year:				
		2019	2018	2017	2016	2015
1	1046.8	1426.6	1475.3	1424.4	1139.5	1672.8
2	1047.0	1442.2	1500.8	1461.9	1185.8	1696.7
3	1028.2	1425.9	1460.0	1439.4	1164.9	1661.9
4	3718.5	5055.3	5267.6	5193.1	4962.0	5511.2

Table 8.17: Mean of number of starts of the fuel cell needed in the MCS (including reactive power consumption of the wind turbine generator).

Case	Measured data from Rye	Data from RenewablesNinja from year:				
		2019	2018	2017	2016	2015
1	222.1	85.9	89.0	75.2	86.5	58.5
2	107.6	36.6	37.9	28.1	31.9	25.6
3	112.9	41.6	52.4	38.7	55.8	29.8
4	4910.0	3573.3	3361.3	3435.0	3666.2	3117.8

The numbers of starts needed in case 4 are, once again, considerably higher than for the rest of the cases. Case 2 seems to need a slightly higher number of starts of the electrolyser, but a significant cut in the number of starts of the fuel cell. Finally, case 3 causes the number of starts to decrease marginally compared to case 1. Nevertheless, the decrease in the number of starts of the fuel cell is more pronounced, almost cutting the number in half at each scenario.

Chapter 9

Discussion

The results presented in the previous chapter give great insight into the performance of the four different control strategies investigated. In this chapter comparisons of the methods used, the performance of the four control strategies and the validity of the results will be conducted.

9.1 Comparison of methods

9.1.1 Analytical method vs. MCS

The two methods presented in chapter 7 yields different results when adequacy assessments are performed using the same input data. This is due to different techniques of calculating the reliability indices. A clear distinction between the analytical method and MCS is the accountability of time. Whilst MCS simulate the events in chronological order, the analytical method does not account for the order which events occur. When analysing the adequacy of a microgrid mainly dependent on fluctuating, renewable power sources, one could argue that this is an obvious weakness in the analytical analysis.

The availability of the resources in the microgrid at Rye is highly time-dependent. The power production of the renewable sources is contingent by the weather, which follows specific patterns during days, weeks and months. Additionally, the energy capacity of the storage units are determined by the amount of surplus or deficit power during the last period. The chronology of events might, therefore, be of more importance when performing an adequacy assessment of a renewable-based microgrid, than in a conventional power grid. Thus, the MCS pose as a better analysing tool than the analytical method in these instances.

The advantage of the time-dependent simulations used in the MCS is apparent when regarding the severity index, EENS. In the analytical method, only the overall probability of load curtailment at different consumption levels is considered. Consequently, the probability of load curtail during periods of low power consumption is minuscule. However, lower consumption levels might trigger load curtail during periods of low power production from the renewable resources and low energy capacity in the storage units. Such instances will be detected by the MCS. Hence one could argue that this approach gives a more accurate estimation of the EENS.

Further, the importance of chronology can be seen in the indices calculated in case 2. Whereas the analytical method only registered cut in load, the MCS, in addition, detected the effect of the load shifting performed by the demand-side management. As can be seen, this leads to a consistent improvement of the adequacy performance of case 2 when using the analytical method. The same improvement can, however, not be detected in the results of the MCS.

The difference between the indices calculated by means of the two methods is noticeable. Wherever the analytical method produces LOLE values far below 1, the LOLE-values calculated by the MCS are in the range 5-7 hrs/yr. A pronounced increase in the EENS calculated by MCS can also be observed. The maximum EENS produced by the analytical method is 13.0694 kWh/yr, while the MCS-EENS-values are about ten times this value.

The adequacy assessment performed by MCS is an HLII-assessment. Hence, the reliability is not only dependent on the availability of the units in the system and the consumption level, but also the availability of the transformers. As these transformers have a low FOR, the effect of unavailability of these components is limited. Thus, the gap between the indices calculated by the two methods can not be explained by the difference in hierarchy level. Though, this does affect the result to some extent.

The indices calculated by the MCS are more pessimistic compared to those of the analytical method.

9.1.2 Impact of reactive power flow

Two MCS were performed, on neglecting and one accounting for the reactive power consumption of the wind turbine generator. The increased energy consumption in the grid causes a slight increase in the LOLP and LOLE indices. This is as expected, as the power production and the availability of the units remain the same.

Nevertheless, the same increase can not be detected in the EENS. Though the expected amount of load curtail does increase in some scenarios, a decrease can be detected in other. The inclusion of reactive power flow causes the load curtails to appear at different instances, sometimes at more ”convenient” occasions, sometimes at less ”convenient” occasions. However, the average EENS does not seem to be heavily affected by the inclusion of reactive power flow.

The small distinctions between the simulations performed with and without accounting for reactive power flow can be explained by the small amount of reactive power consumed by the asynchronous generator. Due to the compensation by the capacitor bank, the reactive power consumption is limited. Furthermore, the reactive power consumption is only present during times of high production levels of the wind turbine. During these hours, there is often surplus energy in the system, increasing the probability of availability of the storage units. Hence, only a minor impact is expected and also observed.

9.2 Evaluation of the four control strategies

The microgrid presented in chapter 2 is a real microgrid, planed to go off-grid in the summer of 2020. To operate the grid in a prudent way the control system described in case 1 is implemented. As case 1 present the actual control logic used at Rye, this case will pose as the base case in the following comparison.

In the following comparison, both the results from the analytical method and the two MCS will be evaluated. Due to the weaknesses of the analytical method and the fact that MCS are more well suited to evaluate microgrids with fluctuating sources, the results from the MCS will be more emphasised hence fort.

9.2.1 Case 2 - Demand-side management

Indices produced by the analytical method indicate a better adequacy performance of the control strategy in case 2 than in the rest of the cases. As discussed previous, this is because only the load shedding is registered by the analytical method. When performing an adequacy assessment by means of MCS, it is shown that case 2 yields slightly higher LOLP and LOLE in 2019, 2018, 2017 and 2016 when no reactive power flow is included, and in 2017, 2016, 2015 and when using measured data in the simulations accounting for the reactive power consumption.

Theoretically, the demand-side management provides an opportunity to increase the adequacy, as load can be moved and peak loads can be cut. Nevertheless, perfect demand-side management is hard to accomplish. When simulating the events in chronological order, the MCS detects the weaknesses in the control logic. The limited flexibility of the loads at Rye causes a less optimal version of demand-side management. Despite the theoretical advantage of flexibility, the control strategy in case 2 also brings about decreased adequacy when implemented at Rye.

Based on the results presented by the MCS, it is hard to evaluate if case 2 pose a better alternative of control strategy. Instances of both increased and decreased LOLP, LOLE and EENS are present.

Further uncertainties can be detected when examining the degradation of the hydrogen system. Despite a decrease in the number of starts needed by the fuel cell compared to case 1, an increased number of starts is needed by the electrolyser. The positive effect of the decrease in fuel cell-starts might, therefore, be cancelled out by the increase of electrolyser-starts. Thus, one can assume that the degradation of the hydrogen system will be similar to that in case 1.

9.2.2 Case 3 - An additional master unit

No distinctions can be found between the adequacy indices for case 1 and 3 calculated by the analytical method. Nevertheless, the two control systems provide different indices in the MCS. A clear answer to which of the two cases that yield the best reliability performance is, though, not clear. In the simulations neglecting the reactive power flow, one can observe that case 3 generally provides lower values of LOLP and LOLE than case 1. This is, however, not the case for the EENS, where the performance of the control strategy seems to vary. The same can be seen in all the indices produced with simulations accounting for the reactive power consumption of the asynchronous generator.

Notwithstanding, a distinction can be observed when looking at the number of starts needed by the components in the HESS. From the simulations, it is evident that the number of starts needed by the fuel cell is significantly lower in case 3 than in case 1. Additionally, a minor reduction in starts needed by the electrolyser can be observed in the simulations disregarding reactive power flow. The same decrease can, however, not be seen when accounting for reactive power.

Consequently, the degradation of the HESS due to start-and-stop cycles is reduced in case 3. It must, nevertheless, be noted that the HESS is forced to operate in load-following mode during times when this unit is acting as the master of the system. The stress added by this kind of operation might, accordingly, increase degradation.

Based on the results provided by the three adequacy assessments conducted, it is hard to determine whether case 3 causes better adequacy performance than case 1. It can, however, be argued that the presence of an extra unit able to act as master in the system will make the microgrid more robust. The control strategy in case 3 allows the microgrid to withstand more faults than that of case 1, and hence the reliability is improved.

9.2.3 Case 4 - Peer-to-peer strategy

When using the analytical method, the results from case 4 stand out when compared to the other cases. The calculated indices indicate considerably worse adequacy during operation with the peer-to-peer control strategy.

The strategy does not, however, yield the same poor results when performing the MCS.

Though the LOLP- and LOLE-values are slightly higher than the other cases, the EENS show a different result. During the simulations, the expected load to be curtailed is lower than the EENS of the other cases. Evidently, the timing of the outages causes the expected load curtailment to decrease compared to case 1, despite an increase in expected hours of outages.

Looking at the results produces from the MCS, it is clear that the peer-to-peer strategy issue increased tear and stress on the HESS. An average of three or four times as many starts are needed of the electrolyser and approximately 25 times as many starts of the fuel cell. In addition, the two units are forced to operate in load-following-mode during operation in case 4. Consequently, the degradation if the HESS is significantly increased in this case and the reliability of the units weakened. In the long run, this could affect the system reliability, as outages of units appear more frequently when entering the wear-out period, cf. the bathtub-curve.

Based on most of the indices presented and the average number of starts needed by the units in the HESS, the peer-to-peer control strategy provides poorer adequacy than the other cases. Nevertheless, the EENSs generated by the MCS indicate the opposite. Additionally, the decentralised control does have certain advantages which are not included in the calculated indices. When solely depending on droop control of local controllers, the system is not dependent on the availability of any master controller nor communication between the resources. Moreover, the load sharing of the units and the distribution of spinning reserve will lead to increased reliability. The advantages of distributed control and spinning reserve can not be quantified in the same manner as the adequacy indices. Thus, it is hard to weigh the strengths and advantages towards each other.

9.2.4 Overall review

From the calculated indices, only small differences between the adequacy of the four control strategies have been detected. One can, however, argue that case 3 provides better reliability than case 1 and 2, as this strategy has included an extra master unit.

In case 1, 2 and 3, the operation of the master controller and means of communication between the resources is vital for proper operation of the microgrid. A system collapse will follow if faults occur at these units.

No master controller nor inter-component-communication are needed during the operation of the microgrid with a peer-to-peer control strategy. Consequently, one could argue that case 4 provides better adequacy than the other cases. Case 4 has, however, presented the most unsatisfactory results when looking at the adequacy indices.

9.3 Evaluation of the system adequacy

Note: When evaluating the adequacy of the microgrid, only the results produced using production data from Rye will be considered. This is because the average production level simulated by RenewablesNinja exceeds that measured at site, and results from assessments using these data might give a falsely positive impression of the adequacy in the microgrid.

With a goal of 98% availability, it is evident that the adequacy is sufficient in all cases investigated. This is despite the fact that the annual energy consumption has increased with approximately 50 MWh since designing the microgrid.

The highest LOLP was calculated to be 0.0774%, from case 4 during MCS including reactive power flow, indicate a security of supply of 99.9226%. This is well within the desired limit. Moreover, the highest EENS detected, from case 2 during the same simulations, was 159.38 kWh/yr. This is equivalent to 0.091% of the annual load, indicating an availability of 99.91%.

Though the REMOTE-goal of 98% availability is reached, it must be notated that the LOLE-values from MCS indicate adequacy below the standard requirement of power system planners, 2.4 hrs/yr. In the four cases, the average LOLE was found to be about 6.3 hrs/yr, equivalent to reliability about two and half time worse than the standard requirement.

9.4 Validity of results

The results produced in this thesis is highly dependent on the access to datasets of production and consumption. These datasets were used as input in the simulations and calculations of the indices. Broader access to historical data would give a more accurate picture of production and consumption patterns at Rye. The limited access to production and consumption data will, thus, affect the validity of the results presented.

The use of simulated production data from RenewablesNinja will, likewise, affect the validity of the results. As mentioned, these data present an average production above the one measured at Rye. Hence, using these data as input might give an inaccurate impression of the reliability performance of the microgrid. It can, however, be argued that as the results only were used to compare possible control strategies in the microgrid, and not to evaluate the adequacy. The increased production level will, thus, have a small impact on the issue discussed in the thesis.

As previously discussed, the analytical method has a significant weakness when not accounting for the chronological order of production and consumption. This weakness is especially pronounced during examinations of the adequacy of systems containing fluctuating, renewable sources. Hence, the validity of the results presented by the analytical

method is weakened.

In the simulations, production and consumption data with a time resolution of one hour was used. A higher time resolution could provide a more detailed description of the performance of the resources in the grid. Furthermore, this would have given more accurate information about the adequacy performance of the microgrid. Thus, a higher time resolution could cause an improvement in the validity of the results.

9.5 Future work

There are several aspects of this thesis that could benefit from further research.

A goal of 98% availability was presented when initiating the microgrid project at Rye. Moreover, the goal of 95% renewable power coverage was also presented. This goal has not been investigated in this thesis. An interesting approach for future work could, therefore, be to investigate how different control strategies contribute to reaching this goal.

Further, in this thesis, a seamless transition from the operation of one master unit to another, during operation with a master-slave control strategy, was assumed. A thorough investigation of the dynamic behaviour of the system during these transformation poses as an intriguing theme for future work.

Finally, further investigation of how the auxiliary energy storage connected to the HESS could contribute to increasing the ramp rate of the HESS must be investigated. How the local control of the HESS should be designed, how big the energy storage must be and how the coupling mechanisms should be designed poses as interesting fields that should be examined in future work.

Chapter 10

Conclusion

The objective of this thesis was to investigate how different control strategies yield different adequacy in an autonomous microgrid. Simulations were executed on an existing microgrid, developed by TrønderEnergi through the REMOTE-project.

Four cases, each presenting a different control strategy, were compared:

- Case 1 - A master-slave control strategy with the BESS as master-unit.
- Case 2 - A master-slave control strategy with the BESS as master-unit and demand-side response.
- Case 3 - A master-slave control strategy with both the BESS and the HESS as master-units.
- Case 4 - A peer-to-peer control strategy.

Using an analytical method, two risk indices, LOLP and LOLE, and one severity index, EENS, were calculated for each of the cases, using six different sets of production data. From the results, it could be observed that case 2 presented the best adequacy performance and case 4 the poorest. Additionally, no distinctions were detected between the performance of case 1 and case 3, though the access to an extra master unit would have a positive impact on the reliability of case 3. Due to the time-independent approach used in the analytical method, the validity of the results produced by this method was found to be weak.

Two types of MCS were performed, one neglecting reactive power and one taking reactive power into account. The results of the two assessments were fairly similar. Case 4 stood out as the case with the highest LOLP- and LOLE-values and the most degradation of the hydrogen system. Case 4 did, however, cause the lowest EENS-values and was the only

control strategy not dependent on a functioning inter-unit-communication system and a master controller. This poses as a huge advantage.

Further, slightly better performance of case 3 was detected. The results did, however, vary in the different simulations performed, and no clear conclusion could be drawn.

The results presented in this thesis are not definite enough to conclude which of the control strategies that ensures the best adequacy performance at Rye. However, the results indicate that all the proposed control strategies would be able to provide an adequacy performance highly sufficient to reach the goal of 98% availability.

Bibliography

[1] Solbes. Systeminformasjon materiell. Unpublished, 2018.

[2] VESTAS. *General Specification VESTAS V27-225kW, 50 Hz Windturbine with tubular/lattice tower*. `http://www.husdesign.no/lars/V27-Teknisk%20spesifikasjon/gen%20specification%20v27.pdf`, January 1994.

[3] Kristian Husmo Lyngved, Thomas Mickelborg, and Anders Teigmoen. Active load management in microgrids. Master's thesis, Norwegian University of Science and Technology, May 2019.

[4] R. Billinton, S. Kumar, N. Chowdhury, K. Chu, K. Debnath, L. Goel, E. Khan, P. Kos, G. Nourbakhsh, and J. Oteng-Adjei. A reliability test system for educational purposes - basic data. *IEEE Transactions on Power Systems*, 4(3):1238–1244, 1989.

[5] R. N. Allan, R. Billinton, J. Sjarief, L. Goel, and K. S. So. A reliability test system for education purposes - basic distribution system data and results. *IEEE Transactions on Power Systems*, 6(2):813–820, 1991.

[6] P. M. Subcommittee. Ieee reliability test system. *IEEE Transactions on Power Apparatus and Systems*, PAS-98(6):2047–2054, 1979.

[7] REMOTE. `https://www.remote-euproject.eu`.

[8] Solbes. Solcellesystem rye - enlinjeskjema. Unpublished, January 2019.

[9] Delphine Wagner, Bernhard Kvaal, Villy Biltoft, and Stefan Knauf. Remote area energy supply with multiple options for integrated hydrigen-based technologies - deliverable number 4.3. Confidential, June 2019.

[10] J. A. Pecas Lopes, C. L. Moreira, and A. G. Madureira. Defining control stategies for microgrids islanded operation. *IEEE transactions on power systems*, 21(3):916–924, May 2006.

[11] Michael Angelo Pedrasa and Ted Spooner. A survey of techniques used to control microgrid generation and storage during island operation. http://citeseerx.ist.psu.edu/viewdoc/download?doi=10.1.1.129.7253&rep=rep1&type=pdf, May 2014.

[12] Karel De Barbandere, Bruno Bolsens, Jeroen Van den Keybus, Achim Woyte, Johan Driesen, and Ronnie Belmans. A voltage and frequency droop control method for parallel inverters. *IEEE transactions on power electronics*, 22(4):1107–1115, July 2007.

[13] Pucheng Pei, Qianfei Chang, and Tian Tang. A quick evaluating method for automotive fuel cell lifetime. *International journal of hydrogen energy*, (33):3829–3836, June 2008.

[14] Roy Billinton and Ronald N. Allan. *Reliability evaluation of power systems*. Plenum Press, second edition edition, 1996.

[15] Anette Solheim. Incorporating demand side response in power system adequacy studies. mathesis, Norwegian University of Science and Technology, June 2019.

[16] Georgia-Ann Klutke, Peter C. Kiessler, and M. A. Wortman. A critical look at the bathtub curve. *IEEE Transactions on Reliability*, 52(1):125–129, March 2003.

[17] Roy Billinton and Bagen. Incorporating well-being considerations in generating systems using energy storage. *IEEE Transactions on Energy Conversion*, 20(1):225–230, March 2005.

[18] Idun Vetvik. Hywind powering utsira. mathesis, Norwegian University of Science and Technology, June 2017.

[19] Ulrikke Bing. System adequacy study of rye microgrid. TET4520 Elektrisk energiteknikk og smarte nett, fordypningsprosjekt.

[20] Horizon2020. What is horizon 2020. https://ec.europa.eu/programmes/horizon2020/what-horizon-2020.

[21] Kyrre Sundseth, Kjetil Midthun, Mats Aarlott, and Adrian Werner. Remote delivrable d2.1 analysis of the economic and regulatory framework of the technological demonstrators. Technical report, REMOTE, 2018.

[22] SolarEdge. Microgrid rye summary report. Unpublished, - -.

[23] Gilert M. Masters. *Renewable and Efficient Electric Power Systems*. IEEE press, 3 edition, 2013.

[24] SolarEdge. Three phase inverter se12.5k - se27.6k. `https://www.solaredge.com/sites/default/files/se-three-phase-inverter-extended-power-datasheet.pdf`, 2019.

[25] Maylis Duru and Trond Rikard Olsen. Site specifications. V2.3, May 2018.

[26] Maylis Duru, Trond Rikard Olsen, Bernhard Kvaal, Villy Biltoft, Stefan Knauf, and Anders Ødegård. Remote area energy supply with multiple options for integrated hydrigen-based technologies - deliverable number 4.1. Confidential, October 2018.

[27] PowiDian. Technical offer - energy storage solution. Technical Proposal ESS Vers: 1, October 2018.

[28] Carmen L. T. Borges and Eduardo Cantarino. Microgrids reliability evaluation with renewable distributed generation and storage system. *IFAC*, 44(1):11695–11700, January 2011.

[29] Claude Lamy. From hrydogen production by water electrolysis to its utilication in a pem fuel cell or in a so fuel cell: Some considerations on the energy efficiencies. *International Journal of Hydrogen Energy*, 41(34):15415–15425, September 2016.

[30] Kohler SDMO. J66k. Technical report, SDMO, Kohler, September 2018. Technocal spesification of generator.

[31] Li Fusheng, Li Ruisheng, and Zhou Fengquan. *Microgrid technology and engineering application*. Elsevier, 2016.

[32] S. Wang, Z. Liu, J. Liu, R. An, and M. Xin. Breaking the boundary: A droop and master-slave hybrid control strategy for parallel inverters in islanded microgrids. In *2017 IEEE Energy Conversion Congress and Exposition (ECCE)*, pages 3345–3352, 2017.

[33] Jan Machowski, Janusz W. Bialek, and James R. Bumby. *Power System Dynamics: Sability and Control*. John Wiley & Sons, 2008.

[34] Farid Katiraei, Reza Iravani, Nikos Hatziargyriou, and Aris Dimeas. Microgrids management: Controls and operation aspects of microgrids. *IEEE power and energy magazine*, 2008.

[35] L van Biert, M. Godjevac, K. Visser, and P. V. Aravind. A review of fuel cwll systems for maritime applications. *Journal of Power Sources*, (327):345–364, July 2016.

[36] Joonas Koponen, Antti Kosonen, Vesa Ruuskanen, Kimmo Houman, Markku Niemelä, and Jero Ahola. Control and energy efficiency of pem water electrolyzers in renewable energy systems. *International journal of hydrogen energy*, (42):29648–29660, October 2017.

[37] Pucheng Pei and Huicui Chen. Main factors affecting the lifetime of proton exchange membrane fuel cells in vehicle applications: A review. *Applied Energy*, (125):60–75, April 2014.

[38] A. Weiß, A. Siebel, M. Bernt, T.-H. Shen, V. Tileli, and H. A. Gasteiger. Impact of intermittent operation on lifetime and performance ofa pemwater electrolyzer. *Journal of the electrochemical society*, 8(166):487–497, 2019.

[39] A. Bergen, L. Pitt, A. Rowe, P. Wild, and N. Djilali. Transient electrolyser responsein a renewable-regenerative energy system. *International journal of hydrogen energy*, (34):64–70, 2009.

[40] Delphine Wagner. Personal communication with delphine wagner from powidian, Autumn 2019.

[41] Wago. Rask kommunikasjon mellom automasjons- og feltenheter: Modbus. https://www.wago.com/no/modbus.

[42] Peter Palensky and Dietmar Dietrich. Demand side management: Demand response, intellegent energy systems, and smart loads. *IEEE transactions on industrial informatics*, 7(3):381–388, 2011.

[43] Dag N. Reppen. Increasing utilization of the transmission grid requires new reliability criteria and comprehensive reliability assessment. *International Conference on Probabilistic Methods Applied to Power Systems, IEEE*, 2004.

[44] Joseph J. Naresky. Reliability definitions. *IEEE Transactions on Reliability*, R-19(4):198–200, November 1970.

[45] Prabha Kundur, John Paserba, Venkat Ajjarapu, Göran Andersson, Anjan Bose, Claudio Canizares, Hatziargyriou, David Hill, Alex Stankovic, Carson Taylor, Thierry Van Cutsem, and Vijay Vittal. Definition and classification of power system stability. *IEEE Transactions on Power Systems*, 19(2):1387–1401, May 2004.

[46] David Elmakias. *New Computational Methods in Power System Reliability*. Springer Berlin Heidelberg, 2008.

[47] Jeongje Park, Wu Liang, Jaeseok Choi, A. A. El-Kaib, Mohammad Shahidehpour, and Roy Billinton. A probabilistic reliability evaluation of a power system including solar/photovoltaic cell generator. *IEEE Power Energy Society General Meeting*, 2009.

[48] Roy Billinton and Kevin Chu. Early evaluation of lolp - evaluating generating capacity requirements. *IEEE power and energy magazine*, pages 88–98, 2015.

[49] Roy Billinton and Wenyuan Li. *Reliability Assessment of Electric Power Systems Using Monte Carlo Methods*. Plenum Press, 1994.

[50] Anniken Auke Borgen. Personal communication with anniken auke borgen from trønderenergi, Autumn 2019.

[51] Stefan Pfenninger and Iain Staffell. Using bias-corrected reanalysis to simulate current and future wind power output. *Energy*, 114:1224–1239, 2016.

[52] Stefan Pfenninger and Iain Staffell. Long-term patterns of european pv output using 30 years of validated hourly reanalysis and satellite data. *Energy*, 114:1251–1265, 2016.

[53] Mostafa Hosseinpour, Habib Rajabi Mashhadi, and Mohammad Ebrahim Hajiabadi. A probabilistic model for assessing the reliability of wind farms in a power system. *JZUS*, 2013.

[54] A. A. Chowdhury. Reliability models for large wind farms in generation system planning. *IEEE Power Engineering Society General Meeting*, 2005.

[55] Kjetil Koldingsnes. Reliability-based derating approach for interconnectors. Master's thesis, Norwegian University of Science and Technology, 2017.

[56] Nina Lindholm. Islanded microgrids: A predicitve approach to control operation. Master's thesis, Norwegian University of Science and Technology, 2020.

Appendices

Appendix A

Data handling

The work presented in this appendix was done in collaboration with Nina Lindholm. A description almost identical to the following chapter might therefore be found in[56]. The collaboration was approved by the supervisors.

A.0.1 Consumption data

Consumption data was collected by gathering data from the different circuits at Langørgen Øvre. However, the hourly consumption data from the circuit in the pigs barn was only saved for three months. Only data from February, Mach and April was available for this circuit. The monthly average was, nevertheless, available for all months over the last year. Consumption levels for the previous months was thereby produced based on the consumption profile from March 2020 multiplied with a factor found based on the monthly average. The monthly average and the factor used can be found in table A.1.

A.0.2 PV-data

Due to faults and maintenance a series of holes were detected in the production data from the PV-system. The following list explains what measures were done to restore the data sets.

- **6/12-19 1:00 - 31/12-19 23:00:** Generated by renewables.ninja, with the MERRA-2 dataset from 2019 with a capacity of 89 kW, a system loss of 5%, a tilt of 35 and an azimuth of 180.
- **1/1-20 00:00 - 9/1-20 13:00:** As little PV-data was available from other sources for

Table A.1: Monthly average consumption and factor multiplied with data from March to generate consumption data from the circuit by the pigs barn.

Month	Monthly average consumption [kW]	Factor
January	2.394	1.257
February	-	Original data used
March	-	Original data used
April	-	Original data used
May	1.230	0.645
June	1.621	0.851
July	1.764	0.926
August	1.941	1.019
September	1.248	0.655
October	0.629	0.330
November	2.055	1.079
December	2.173	1.140

2020 and this period was rather short, the first nine days of January 2020 were filled in with data from 10/1-20 00:00 - 19/1/20 13:00.

- **30/1-20 13:00 - 5/2-20 8:00:** For most of this period, the measured temperature and irradiance was available. Using a machine learning model built on previous data (april-november) by Nina Lindholm [56], the power output of the panels was predicted.
- **4/2-20 16:00 - 5/2-20 8:00:** The datapoints were substituted with the values from the following day.
- **Minor holes:** A number of smaller holes were found, typically 1-7 hours missing at a time. These were 8/10-19 09:00-12:00, 22/2-20 12:00-18:00, 28/3-20 11:00 and 29/3-20 02:00. As these were limited in timespan it was decided that the power was replaced by a linear function between the previous and coming data points.

A.1 Wind-data

The wind measurements were made with 10 minute intervals, all on the wind turbine. To make a coherent datasets several measurements had to be fixed. First, all duplicates were removed. Thereafter, all the datapoints were analysed to replace missing values. When the missing values covered a time less than four hours, they were replaced by a linear function between the previous and coming data points. With gaps larger than four hours the values were replaced by the values of the previous day. Thereafter all the 10 minutes measurements were averaged in order to make up an hourly dataset.

The data points that had to be replaced were:

- **Linear replacement:**
  - 1/4-19 23:50 - 2/4-19 00:50
  - 11/4-19 10:30
  - 25/5-19 11:00
  - 23/10-19 10:10-10:20
  - 12/11-19 11:00-11:20
  - 11/12-19 2:20-3:30
  - 11/12-19 3:40-4:40
  - 11/12-19 10:40
  - 17/1-20 12:00-12:10
  - 20/1-20 16:20
  - 31/1-20 11:30-11:40
- **Replaced by previous:**
  - 8/10-19 9:00-12:50
  - 8/10-19 13:00 - 9/10-19 12:20
  - 10/12-19 19:10-22:00
  - 1/1-20 5:00-9:40
  - 4/1-20 3:00-8:20
  - 4/2-20 15:40 - 4/2-20 9:20
  - 22/2-20 12:20-19:00

Appendix B

Algorithms of LOLE and EENS

B.1 Algorithm used to calculate LOLE when using the analytical method

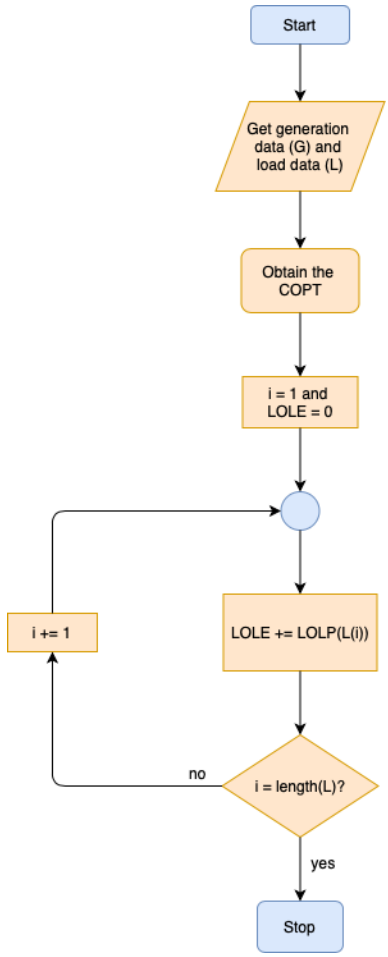

Figure B.1: The algorithm used to calculate the LOLE when using the analytical method.

B.2 Algorithm used to calculate EENS when using the analytical method

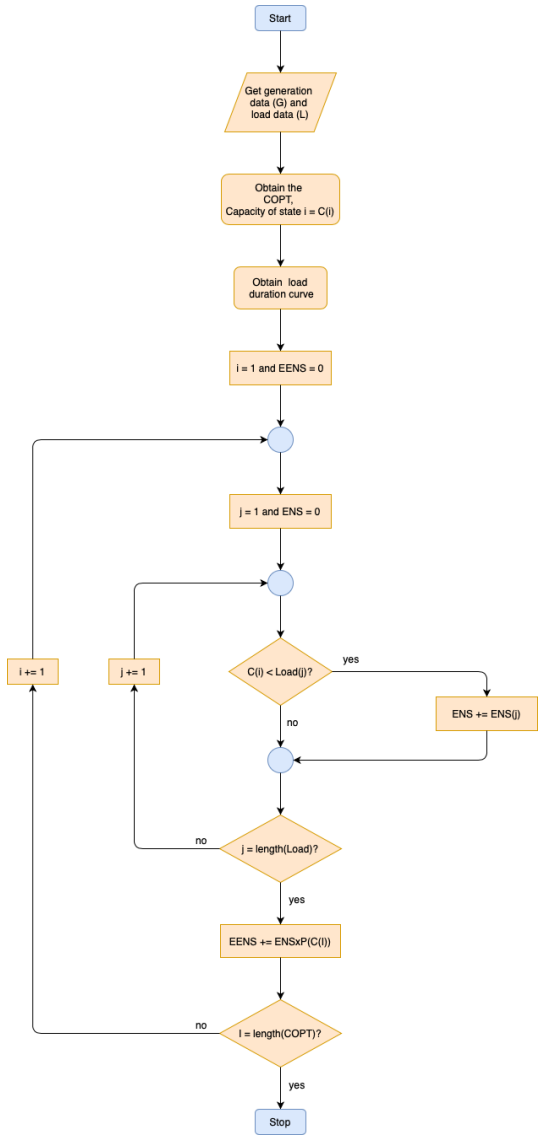

Figure B.2: The algorithm used to calculate the EENS when using the analytical method.

Appendix C

COPTs used in the HLI adequacy assessment using an analythical method

C.1 Renewable sources

Table C.1: COPTs of the PV-system using a seven-state model.

			Probability					
State	**Capacity In [kW]**	**Capacity Outage [kW]**	**Measured data from Rye**	**Data from RenewablesNinja from year:**				
				2019	**2018**	**2017**	**2016**	**2015**
1	82.8	0	0.0001	0.0031	0.0066	0.0049	0.0028	0.0017
2	74.52	8.28	0.0179	0.0340	0.0326	0.0271	0.0282	0.0231
3	57.96	24.84	0.0349	0.0413	0.0378	0.0454	0.0455	0.0412
4	41.4	41.4	0.0485	0.0561	0.0598	0.0589	0.0597	0.0539
5	24.84	57.96	0.0717	0.0837	0.0906	0.0859	0.0900	0.0884
6	8.28	74.52	0.3284	0.2590	0.2539	0.2541	0.2512	0.2682
7	0	82.8	0.4985	0.5229	0.5186	0.5236	0.5226	0.5237

Table C.2: COPTs of the wind turbine using a seven-state model.

			Probability					
State	**Capacity In [kW]**	**Capacity Outage [kW]**	**Measured data form Rye**	**Data from RenewablesNinja from year:**				
				2019	**2018**	**2017**	**2016**	**2015**
1	225	0	0.0007	0.0000	0.0000	0.0000	0.0000	0.0000
2	202.5	22.5	0.0122	0.0000	0.0000	0.0000	0.0006	0.0000
3	157.5	67.5	0.0226	0.0100	0.0039	0.0015	0.0015	0.0076
4	112.5	112.5	0.0401	0.0232	0.0128	0.0167	0.0113	0.0418
5	67.5	157.5	0.0818	0.0676	0.0791	0.1017	0.0831	0.1106
6	22.5	202.5	0.3731	0.6870	0.6994	0.6866	0.6987	0.6577
7	0	225	0.4694	0.2123	0.2048	0.1935	0.2049	0.1822

C.2 Storage units in case 1

Table C.3: COPTs of the BESS using a four-state model for case 1.

			Probability					
State	**Capacity In [kW]**	**Capacity Outage [kW]**	**Measured data form Rye**	**Data from RenewablesNinja from year:**				
				2019	**2018**	**2017**	**2016**	**2015**
1	216	0	0.6961	0.8600	0.8748	0.8698	0.8589	0.8871
2	144	72	0.1251	0.0637	0.0600	0.0766	0.0826	0.0706
3	72	144	0.1717	0.0660	0.0554	0.0439	0.0485	0.0328
4	0	216	0.0107	0.0104	0.0098	0.0097	0.0100	0.0095

Table C.4: COPTs of the HESS using a four-state model for case 1.

			Probability					
State	**Capacity In [kW]**	**Capacity Outage [kW]**	**Measured data form Rye**	**Data from RenewablesNinja from year:**				
				2019	**2018**	**2017**	**2016**	**2015**
1	100	0	0.7663	0.8955	0.9172	0.9264	0.9193	0.9319
2	66.66	33.33	0.0158	0.0087	0.0012	0.0016	0.0051	0.0007
3	33.33	66.66	0.1899	0.0008	0.0007	0.0017	0.0048	0.0393
4	0	100	0.0281	0.0950	0.0809	0.0704	0.0708	0.0281

C.3 Storage units in case 2

Table C.5: COPTs of the BESS using a four-state model for case 2.

			Probability					
State	**Capacity In [kW]**	**Capacity Outage [kW]**	**Measured data form Rye**	**Data from RenewablesNinja from year:**				
				2019	**2018**	**2017**	**2016**	**2015**
1	216	0	0.6986	0.8657	0.8773	0.8692	0.8591	0.8874
2	144	72	0.1222	0.0606	0.0580	0.0783	0.0912	0.0731
3	72	144	0.1696	0.0643	0.0553	0.0432	0.0405	0.0300
4	0	216	0.0097	0.0095	0.0093	0.0093	0.0092	0.0096

Table C.6: COPTs of the HESS using a four-state model for case 2.

			Probability					
State	**Capacity In [kW]**	**Capacity Outage [kW]**	**Measured data form Rye**	**Data from RenewablesNinja from year:**				
				2019	**2018**	**2017**	**2016**	**2015**
1	100	0	0.7669	0.8961	0.9274	0.9272	0.9244	0.9321
2	66.66	33.33	0.0210	0.0087	0.0011	0.0061	0.0058	0.0051
3	33.33	66.66	0.1840	0.0012	0.0007	0.0386	0.0417	0.0347
4	0	100	0.0281	0.0940	0.0808	0.0281	0.0218	0.0218

C.4 Storage units in case 3

Table C.7: COPTs of the BESS using a four-state model for case 3.

			Probability					
State	**Capacity In [kW]**	**Capacity Outage [kW]**	**Measured data form Rye**	**Data from RenewablesNinja from year:**				
				2019	**2018**	**2017**	**2016**	**2015**
1	216	0	0.6961	0.8600	0.8748	0.8698	0.8589	0.8871
2	144	72	0.1251	0.0637	0.0600	0.0766	0.0826	0.0706
3	72	144	0.1717	0.0660	0.0554	0.0439	0.0485	0.0328
4	0	216	0.0107	0.0104	0.0098	0.0097	0.0100	0.0095

Table C.8: COPTs of the HESS using a four-state model for case 3.

			Probability					
State	**Capacity In [kW]**	**Capacity Outage [kW]**	**Measured data form Rye**	**Data from RenewablesNinja from year:**				
				2019	**2018**	**2017**	**2016**	**2015**
1	100	0	0.7663	0.8955	0.9172	0.9264	0.9193	0.9319
2	66.66	33.33	0.0158	0.0087	0.0012	0.0016	0.0051	0.0007
3	33.33	66.66	0.1899	0.0008	0.0007	0.0017	0.0048	0.0393
4	0	100	0.0281	0.0950	0.0809	0.0704	0.0708	0.0281

C.5 Storage units in case 4

Table C.9: COPTs of the BESS using a four-state model for case 4.

			Probability					
State	**Capacity In [kW]**	**Capacity Outage [kW]**	**Measured data form Rye**	**Data from RenewablesNinja from year:**				
				2019	**2018**	**2017**	**2016**	**2015**
1	216	0	0.7058	0.8730	0.8542	0.8746	0.8657	0.8772
2	144	72	0.0663	0.0245	0.0324	0.0337	0.0397	0.0336
3	72	144	0.0652	0.0336	0.0396	0.0426	0.0379	0.0398
4	0	216	0.1627	0.0688	0.0639	0.0490	0.0567	0.0494

Table C.10: COPTs of the HESS using a four-state model for case 4.

			Probability					
State	**Capacity In [kW]**	**Capacity Outage [kW]**	**Measured data form Rye**	**Data from RenewablesNinja from year:**				
				2019	**2018**	**2017**	**2016**	**2015**
1	100	0	0.7354	0.8923	0.9214	0.9121	0.9116	0.9346
2	66.66	33.33	0.0232	0.0057	0.0028	0.0091	0.0065	0.0017
3	33.33	66.66	0.0514	0.0206	0.0083	0.0255	0.0148	0.0125
4	0	100	0.1900	0.0814	0.0675	0.0533	0.0671	0.0512

Ulrikke Bing

Microgrid Control: The impact of different control strategies on the system adequacy

NTNU
Norwegian University of
Science and Technology

TrønderEnergi